AN ABSTRACT OF THE THESIS OF

Gannavaram D. Vishakhadatta for the degree of Master of Science in Electrical and Computer Engineering presented on April 1, 1993

Title: Finite Element Modeling of Dielectric Waveguides

Abstract approved: Redacted for Privacy

Thomas K. Plant

Dielectric waveguides are becoming important for their numerous applications in integrated optics. The study of dielectric waveguides by analytical techniques is not sufficient for many variations in waveguide shape, anisotropy, and inhomogeneity commonly encountered in waveguide materials. This work studies the finite element method as an accurate tool for the numerical modeling of dielectric waveguides. Other commonly used numerical techniques are also considered. The implementation of the finite element method is discussed. The finite element technique is also modified to incorporate the lack of fixed-potential boundary conditions in dielectric waveguides. The results of the simulations are documented for several experimental and analytical test cases.

Measurements were made on waveguides fabricated in-house using the plasma-enhanced chemical vapor deposition (PECVD) films of silicon oxynitride. The light source was a 6328 Å helium-neon laser. The results of the finite element simulations are compared with the experimental results and with other previously documented numerical and analytical results from the literature. The finite element method developed here is shown to be in good agreement with these results and will be useful in solving for the modes of novel waveguide designs.

Finite Element Modeling of Dielectric Waveguides

by

Gannavaram D. Vishakhadatta

A THESIS

submitted to

Oregon State University

in partial fulfillment of
the requirements for the
degree of

Master of Science

Completed April 1, 1993

Commencement June 1993

APPROVED:

Redacted for Privacy

Professor of Electrical and Computer Engineering in charge of major

Redacted for Privacy

Head of Department of Electrical and Computer Engineering

Redacted for Privacy

Dean of Graduate School

Date thesis is presented April 1, 1993

Typed by Gannavaram D. Vishakhadatta

ACKNOWLEDGMENT

I am very grateful to my advisor, Dr. Thomas Plant, for his guidance and encouragement during the course of my studies at Oregon State. I would also like to thank him for the financial support that he lent me at a crucial time.

I would like to thank Sungkyoo Lim for his ready help in the growth of the dielectric waveguides and Kate Remley for her help in verifying my simulations. I am also grateful to Professors Vijai Tripathi and Andreas Weisshaar for their critical advice and guidance during the course of my research work.

Table of Contents

List of Figures

List of Tables

FINITE ELEMENT MODELING OF DIELECTRIC WAVEGUIDES

1. INTRODUCTION

Recently, integrated optoelectronic systems have been proposed to achieve faster and more reliable computing and data processing. Both applications involve the switching and modulation of optical beams. The advantage of integrated optics over conventional electronics is the high degree of parallelism possible in the digital processing of optical signals. Integrated optical structures also make use of natural optical anisotropies and non-linearities. Anisotropic materials display a refractive index that depends on the polarization and direction of propagation of an optical beam through the material. The refractive index of non-linear materials depends on the strength of any externally applied fields and the strength of the optical signal itself. Such properties can be implemented to design optical modulators, switches and phase shifters that are crucial to integrated optical computing applications.

Dielectric optical waveguides form the basis of all optoelectronic structures. They are crucial as a means of connecting various active optical devices. They are also applicable as devices such as 3 dB power splitters, which utilize the field interactions of waveguides in close proximity, and optical switches and amplifiers that are directly implemented on a waveguide structure. Dielectric waveguides are quite unlike conventional microwave waveguides as they do not possess any fixed boundary potentials and usually possess many small variations in size and shape as a result of tolerances in fabrication on such a small scale (in the range of hundreds of angstroms).

1.1 MOTIVATION

The design of optoelectronic systems and active integrated optic devices requires an understanding of the field distributions and the modal waveguiding properties of dielectric optical waveguide structures. Such devices are likely to incorporate many different characteristics like anisotropies, nonlinearities and unconventional waveguide designs. Analytical techniques normally used in simple dielectric waveguide analysis do not meet the demands of such complex structures. Numerical techniques are often able to accurately approximate the actual characteristics of such devices. A reliable numerical technique must be developed to enable the study of such structures. The finite element method is extremely suitable to study dielectric waveguide structures due to its ability to handle unconventional systems. This method is also suitable for the study of structures without fixed boundary conditions as in the case of dielectric waveguides. In this work, we address the various parameters that a numerical technique should meet to be suitable for application to dielectric waveguide analysis and study the utility of the finite element method in such an application by comparing the results of the finite element simulations with experiments and other previously documented results.

1.2 SYNOPSIS OF CHAPTERS

In chapter two, the theory and properties of dielectric waveguides are discussed. Various numerical techniques are described and the finite element method of numerical analysis is analyzed as a versatile tool for the study of dielectric waveguides.

In chapter three, the actual implementation of the finite element method to dielectric optical waveguides is developed. Various methods by which the finite

element formulation can be implemented are also examined. The scope of the problem is expanded to handle material anisotropy and variations in refractive index profile.

Chapter four describes the fabrication and measurement of several test waveguides to compare with the model. Chapter five examines the results of the finite element simulations and compares them with previously published results and with experimental data. The utility of the finite element method is examined in light of these comparisons and possibilities for future work are proposed.

2. THEORY OF DIELECTRIC WAVEGUIDE SOLUTIONS

In this chapter, we discuss the theory of optical wave propagation in dielectric waveguides. We also introduce the various terms that are used to characterize the propagation of light in dielectric waveguides.

2.1 TERMINOLOGY

Dielectric waveguides consist of an area of higher refractive index that is surrounded by materials of lower refractive indices. The materials are required to possess a high degree of transparency to light at the wavelengths of interest which enables the light to propagate in the waveguide for long distances. The simplest dielectric waveguides consist of an infinite slab of a certain thickness surrounded by a cover layer and a substrate layer, as shown in figure 2.1.

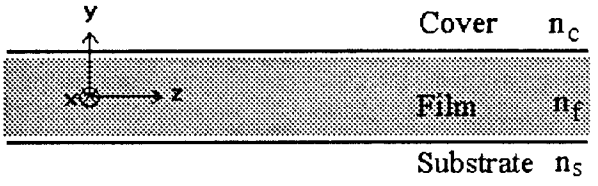

FIGURE 2.1 Dielectric Slab Waveguide

The profile of the refractive index may vary across the cross section of the film layer. Waveguides which have a uniform index of refraction across the film are known as homogenous slab waveguides. Waveguides whose refractive index

varies as a function of depth in the film are called inhomogenous waveguides. The slab waveguide is known as a symmetrical slab waveguide when the refractive index of the cover layer is the same as that of the substrate layer. If the refractive indices of the cover and substrate are different, then the waveguide is called an asymmetric slab waveguide. The layers of the waveguide might also be anisotropic, i.e., possess a refractive index that is dependent on the direction of polarization of light in the medium.

The phenomenon of total internal reflection occurs when light traveling in a medium of higher refractive index is incident on the dielectric interface with a medium of lower refractive index at an angle greater than the critical angle as shown in figure 2.2. The critical angle θ_c of a dielectric interface is that angle of incidence at which the beam refracted into the medium of lower refractive index travels along the dielectric interface. Light incident at an angle greater than the critical angle is completely reflected back into the higher index material. Light propagates in the waveguide by total internal reflection at the dielectric interfaces.

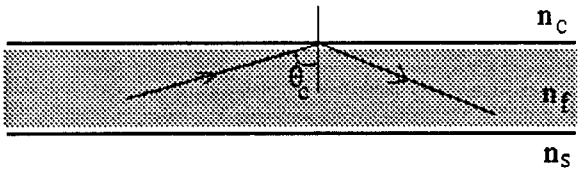

$$\theta_c = \sin^{-1}(n_c / n_f)$$

Figure 2.2 Critical Angle at a dielectric interface

The waveguide is only able to support the propagation of a beam of light when the wavefront travels at particular angles to the longitudinal propagation direction. At these angles, the beam tends to constructively interfere with itself. At all other angles, the beam destructively interferes with itself, resulting in no propagation. Each individual allowed propagation angle is called a "mode" of the waveguide.

All possible allowed modes in the waveguide, incident at the dielectric interface at an angle greater than the critical angle of the dielectric interface, will be supported. Any light incident on the dielectric interface at angles less than the critical angle is no longer confined to the waveguide and is lost in the transverse direction by transmission into the cladding.

The allowed modes in the waveguide can be further classified according to the polarization directions of the electric and magnetic fields of the waves in the waveguides. Modes that possess an electric field **E** purely perpendicular to the direction of propagation in the waveguide are called Transverse Electric (TE) modes. The magnetic intensity **H** of such modes has components both perpendicular to and along the direction of propagation.

Modes that possess a magnetic intensity **H** purely perpendicular to the direction of propagation in the waveguide are known as Transverse Magnetic (TM) modes. Such modes possess an electric field **E** with components both perpendicular to and along the direction of propagation.

2.2 PROPAGATION IN DIELECTRIC WAVEGUIDES

In determining the waveguiding properties of the dielectric slab waveguide, we obtain the different modes that propagate at given frequencies and their propagation constants. For the asymmetric slab dielectric waveguide represented

in Figure 2.1, the film itself has a refractive index, n_f, higher than that of the refractive indices of the cover, n_c, or the substrate, n_s. The propagating modes are well confined to the film, with exponentially decaying fields in the cover and substrate regions, as shown in Figure 2.2. The longer evanescent "tail" into the substrate is due to the smaller dielectric constant mismatch of n_f and n_s than of n_f and n_c.

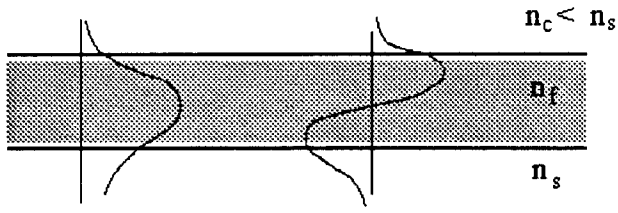

FIGURE 2.3 Well - confined modes in a waveguide

Here, we assume that $n_s > n_c$. (In many cases, the cover is air so $n_c = 1$). Modes that do not propagate "leak" into the cover and/or substrate with propagation perpendicular to the dielectric interface, as represented in Figure 2.4.

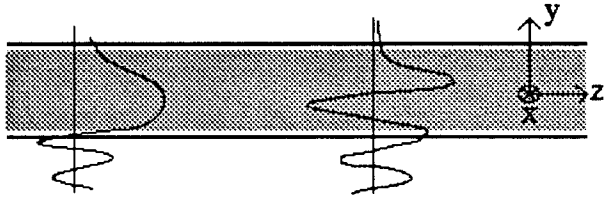

FIGURE 2.4 Unconfined modes leak into the substrate

For waves propagating along the z direction, the fields in the waveguide are given, excluding the exp(jωt) time dependence, as

$$\mathbf{H} = \mathbf{H}(y) \,.\, \exp(-j\beta z) \tag{2.1}$$

$$\mathbf{E} = \mathbf{E}(y) \,.\, \exp(-j\beta z) \cdot \tag{2.2}$$

There is no field dependence in the x direction since the waveguide is assumed infinite along the x axis.

From Maxwell's equations, when $\mathbf{J} = 0$,

$$\nabla \mathrm{X}\, \mathbf{E} = -\mathrm{j}.\omega.\mu_0.\boldsymbol{\mu}_r.\mathbf{H} \tag{2.3}$$

$$\nabla \mathrm{X}\, \mathbf{H} = \mathrm{j}.\omega.\varepsilon_0.\boldsymbol{\varepsilon}_r.\mathbf{E} \tag{2.4}$$

where $\boldsymbol{\mu}_r$ and $\boldsymbol{\varepsilon}_r$ are, respectively, the tensor relative permeability and relative permittivity of the general anisotropic dielectric medium. In order to constitute a propagating wave, equations 2.1 and 2.2 must satisfy equations 2.3 and 2.4 and the boundary conditions in the entire dielectric space.

For isotropic media, the tensor quantities $\boldsymbol{\varepsilon}_r$ and $\boldsymbol{\mu}_r$ become scalar constants, i.e., $\boldsymbol{\varepsilon}_r = \varepsilon_r$ and $\boldsymbol{\mu}_r = \mu_r$, and equations 2.3 and 2.4 become, by taking the curl of one, substituting the other, and using the vector identity for $\nabla \mathrm{X} \nabla \mathrm{X}\, \mathbf{E}$,

$$\nabla_t^2.\mathbf{H} + (k^2 - \beta^2).\mathbf{H} = 0 \tag{2.5}$$

$$\nabla_t^2.\mathbf{E} + (k^2 - \beta^2).\mathbf{E} = 0 \tag{2.6}$$

where $k = k_0 n$ is the wave number of the propagating wave,

$k_0 = (2\pi / \lambda_0)$,

∇_t^2 is the transverse Laplacian operator

and $n = \sqrt{\varepsilon_r}$.

The practical problem posed is to determine the finite set of propagation constants that can exist in the waveguide for a given value of the wave number.

The set of propagation constants β_i correspond to the allowed modes of the waveguide. Only positive values of β_i imply guided waves.

Another parameter commonly dealt with in the study of propagation in waveguides is the "effective index" of the waveguide, N_{eff}, given by (β / k_0). The effective index is also known as the normalized propagation constant, N_{eff}.

For a propagating mode as shown in Figure 2.3,

$$k_y^2 + k_z^2 = k^2 \tag{2.7}$$

$$k_z = \beta, \quad \text{the longitudinal propagation constant} \tag{2.8}$$

$$\text{i.e.,} \quad k_y^2 + \beta^2 = k_0^2 . n_f^2 \tag{2.9}$$

$$\text{i.e.,} \quad 0 \leq \beta \leq k_0 . n_f \tag{2.10}$$

For a wave polarized in the x - direction and propagating in a medium of infinite extent ($\lambda << d$, the waveguide thickness) with refractive index n_x, $k_y = 0$ and the wave is a plane TEM wave in the absence of any boundaries and the propagation constant is given by $\beta = (2.\pi.n_x / \lambda_0)$. The effective index is now $N_{eff} = n_x$.

In a waveguide of finite thickness($\lambda \sim d$), the mode is not entirely confined to the waveguide itself. The evanescent wings of the mode extend into the cover and substrate. Thus, for propagating modes in the waveguide, N_{eff} has a value higher than n_c and n_s, and lower than n_f. The mode is thus effectively traveling in a medium whose refractive index is higher than that of the cover and substrate, i.e., the wave is primarily confined to the film. At very high values of β, the value of N_{eff} approaches that of n_f. The ratio N_{eff} / n_f is a measure of how well the mode is confined in the film. "Well confined" modes have very small evanescent field "tails" in the surrounding cover and substrate materials. The ratio approaches 1 for very highly confined modes.

Another important aspect of the modal solutions for dielectric waveguides is the distribution of the electric and magnetic fields inside the waveguides and in the substrate and cover layers. The optical power is proportional to the square of the transverse electric field. The waveguide field distribution is easily determined for a given β and N_{eff} as solutions to equations 2.1 through 2.4 over the area of interest.

2.3 MODELING OF DIELECTRIC WAVEGUIDES

Most of the techniques, such as the finite difference method and the transmission line method, used in the modeling of microwave waveguide problems are quite unsuitable for application to dielectric waveguides due to the absence of any fixed boundary conditions. The principal techniques applicable to dielectric waveguides are represented below.

2.3.1 The Direct Matching Method

The use of the boundary value method is very suitable in dealing with multi layer dielectric waveguides. The propagating beam is assumed to possess a certain distribution in the various layers. In the case of the slab dielectric waveguide, the beam is assumed to possess an exponential decay in the cover and substrate layers and a suitable distribution in the film layer. The parameters of the distribution are solved by implementing the boundary conditions at the interfaces. The applicable boundary conditions in this case are

$$E_{t1} = E_{t2} \tag{2.11}$$

$$D_{n1} = D_{n2} \qquad [\rho_s = 0] \tag{2.12}$$

$$H_{t1} = H_{t2} \qquad [J_s = 0] \tag{2.13}$$

$$B_{n1} = B_{n2} \tag{2.14}$$

where the subscript "t" indicates the components tangential to the dielectric interface while the subscript "n" indicates the components normal to the dielectric interface. The choice of the distribution chosen in the layers implies the presence of either a TE or a TM solution. Thus, this method cannot handle hybrid solutions present in certain waveguide cases, where the modes are neither pure TE nor pure TM solutions [1]. In addition, the method is quite cumbersome to use for inhomogenous dielectric waveguides, such as a nonuniform distribution of refractive index in the film layers.

2.3.2 The Geometrical Ray Propagation Method

The beam propagation method is extremely convenient for dealing with propagation through dielectric layers. Each layer is treated as an impedance in a transmission line problem. The problem thus reduces to a set of connected transmission lines. However, this method is not suitable for the study of inhomogenous dielectric waveguides.

2.3.3 The Finite Element Method

In the finite element method, the problem area is discretized in space into elements of finite length. A suitable field distribution is assumed in each of the finite elements as an interpolation of the field intensities at the nodes of the element. A variational function representing an "error" of the calculated field over the actual field is calculated over each of the individual elements. Variational functions are given in terms of the field distribution of the problem and a minimization of the variational function implies the distribution of the fields in the problem satisfies Maxwell's equations, equations 2.3 and 2.4. The variational functions calculated for each of the elements of the problem are linked to set up the whole problem by linking the fields of the elements at the common nodes they

share. The minimization of the variational function now yields a distribution of the fields at the nodes which can be used to determine the fields throughout the problem by interpolating the values of the fields at the nodes of each element.

The analysis of dielectric waveguides using the boundary value method cannot easily accommodate inhomogeneities and anisotropies in the waveguide. The finite element method can be made to include anisotropy in the waveguides by choosing tensor permittivities of the waveguide and cladding. Waveguide inhomogeneities can also be incorporated by choosing an appropriate interpolation of the values of the refractive index in each of the elements. The finite element method is also very advantageous in certain cases where the resultant solutions tend to be other than pure TE and TM solutions as there is no implicit assumption that the solutions are purely TE or TM solutions.

2.4 BACKGROUND

A comprehensive guide to the theory of dielectric waveguides is provided by Marcuse[2]. Cherin[3] discusses in detail the analytical solutions for symmetric, isotropic cases. However, analytical techniques are quite unsuitable for inhomogenous and anisotropic cases commonly encountered. The use of numerical techniques has been suggested as a feasible alternative in such cases.

Although the finite element problem can be set in numerous ways, Itoh [4] suggests that there are strong advantages to using a variational formulation. In addition to being able to set up the problem more efficiently, the variational formulation lends itself to the methodical and quick setting up of the perturbation theory and its applications in the analysis of minute perturbations to a standard problem.

The variational functions can be set up in terms of the scalar fields of the problem [5] or described in terms of the complete or partial vector fields of the problem [6,7,8]. Berk [7] explains the variational formulae useful for electromagnetic problems in terms of the more complete **E** or **H** vector notation. The methods of derivation of variational formulations are also dealt with in detail and the formulations are also applied to the derivation of perturbation formulas.

Silvester and Ferrari [1] and Silvester and Chari [9] discuss various methods of discretizing the problem. The process of assembling the finite element problem is also dealt with. Itoh [4] also discusses the usage of artificially imposed boundary conditions to denote symmetry in the problem.

Spurious field distributions may appear in solutions to variational formulations using vector fields [8,10]. Bardi and Biro [11] discuss finite element formulations for dielectric waveguides that eliminate the presence of spurious modes. The penalty function method is introduced [12,13,14] as a method to eliminate spurious solutions. By implementing the Coulomb gauge for **H**, i.e., by implying $\nabla.\mathbf{H} = 0$, spurious solutions are made less significant.

The setting up of artificial boundary conditions to limit the scope of the problem and to provide approximate solutions has been suggested by Mabaya, Lagasse and Vandenbulcke [15]. The fields are assumed to die out completely a sufficient distance from the waveguide where the imposition of a Dirichlet or Neumann condition reduces the tangential vector electric and magnetic fields to zero. This method requires intense computational resources as it involves the extension of the regular finite element problem considerably farther from the area of interest which reduces the accuracy available. In addition, the solutions in the waveguide can only be considered approximations due to the curtailing of the fields occurring at the artificial boundaries. The validity of such solutions is

shown by imposing the conditions at various distances from the waveguide and arriving at an invariant solution.

Rahman and Davies [16,17] suggest the use of infinite elements to completely describe the fields present in the cover and substrate. The use of infinite elements enables an accurate modeling of the evanescent fields while preserving the computation required. The solution to the problem has been shown to depend very weakly on the magnitude of the constant of exponential decay. In addition, the decay length has been shown to be a derivable solution of the eigenvalue problem.

3. THE FINITE ELEMENT METHOD

3.1 THE VARIATIONAL FORMULATION

3.1.1 Choice of fields

The implementation of the variational formulation can be carried out using methods such as a scalar field implementation [5], using the axial fields of **E** and **H** [8], the transverse fields of **E** and **H** [6] or by utilizing the more complete **E** or **H** field descriptions. General dielectric waveguide solutions are distortions of pure TE and TM solutions and contain both E_z and H_z field components. They are, consequently, referred to as hybrid modes. Hybrid modes arise out of a "mixing" of the TE and TM modal solutions which is caused by the dielectric inhomogeneity. As a result, accurate numerical formulations need to use at least 2 independent field components [1]. Although infinite slab dielectric waveguides demonstrate pure TE and TM solutions, the generalized formulation helps us get a better understanding when we encounter waveguide structures with hybrid modes.

The boundary conditions to be satisfied at the dielectric interface are

$$E_{t1} = E_{t2} \tag{3.1.1}$$

$$D_{n1} = D_{n2} \qquad [\rho_s = 0] \tag{3.1.2}$$

$$H_{t1} = H_{t2} \qquad [J_s = 0] \tag{3.1.3}$$

and

$$B_{n1} = B_{n2}. \tag{3.1.4}$$

where the subscript "t" indicates the components tangential to the dielectric interface while the subscript "n" indicates the components normal to the dielectric interface.

Abrupt changes in the permittivity, ε_r, are encountered as we cross the dielectric interface. Hence, any field solution may not be continuous in **E** [21].

As a rule, μ_r is 1.0 in dielectric media. This means that at the dielectric interface, equation 3.1.4 simplifies to

$$H_{n1} = H_{n2} \tag{3.1.5}$$

Hence, throughout the dielectric problem, **H** is continuous in the absence of a surface current. Thus, it is much more convenient to set up the variational formulation in terms of **H**.

Although it is sufficient to set up the problem in terms of the H_x and H_y components alone, we choose to formulate the problem using all 3 **H** components so as to be able to obtain a complete vector solution [7].

3.1.2 Variational Equation

In the previous chapter, we have discussed the utility of a variational formulation in generating the finite element problem. The variational formulation that we choose to adapt to the finite element formulation of lossless dielectric problems is [4]

$$\omega^2 = SV \iint \frac{\left[(\nabla XH)^*.\hat{\varepsilon_r}^{-1}.(\nabla XH)\right]}{\left[H^*.\hat{\mu_r}.H\right]}.dx.dy \tag{3.1.6}$$

where SV stands for stationary value with respect to H.

This formulation yields stationary values of ω^2 when the condition

$$\nabla X (\varepsilon_r^{-1}.\nabla X \mathbf{H}) - \omega^2.\mu_r.\mathbf{H} = 0 \tag{3.1.7}$$

is satisfied [4].

For the isotropic case, $\varepsilon_r = \varepsilon_r$ and $\mu_r = \mu_r$ and equation 3.1.7 simplifies to

$$\nabla^2\mathbf{H} + k^2.\mathbf{H} = 0. \tag{3.1.7a}$$

The fields that satisfy this functional are defined by

$$\mathbf{n} X \delta\mathbf{E} = 0 \tag{3.1.8}$$

where **n** is the normal to the dielectric interface. That is, the tangential electric field, (**n** X **E**) is continuous. However, the field is not required to satisfy the boundary condition

$$\mathbf{n} \times (\varepsilon_r^{-1} . (\nabla \times \mathbf{H})) = 0$$

since the tangential electric fields do not vanish at the dielectric interface as in the case of metallic waveguides. The anisotropy of the waveguide is described by the tensor permittivity and permeability which are assumed real, i.e., the media are assumed to be lossless.

To facilitate the interpretation of the above variational functional numerically, we modify it so that

$$J = SV \iint \left[(\nabla \times \mathrm{H})^* . \hat{\varepsilon}_r^{-1} . (\nabla \times \mathrm{H}) - k^2 \mathrm{H}^* . \hat{\mu}_r . \mathrm{H} \right] dx . dy \qquad (3.1.9)$$

The solutions of equation 3.1.9 sometimes result in the presence of spurious solutions that numerically satisfy the equation but are not physical waveguide solutions [12,13]. The spurious modes violate Maxwell's equations by not satisfying $\nabla . \mathbf{H} = 0$. Hence, we modify Equation 3.1.9 with a penalty condition so that the formulation now is

$$J = SV \iint \left[(\nabla \times \mathrm{H})^* . \hat{\varepsilon}_r^{-1} . (\nabla \times \mathrm{H}) - k^2 . \mathrm{H}^* . \hat{\mu}_r . \mathrm{H} + \alpha . (\nabla . \mathrm{H})^* . (\nabla . \mathrm{H}) \right] dx . dy \qquad (3.1.10)$$

where α is a positive, arbitrary penalty constant. The effect is that for spurious solutions, the value of the variational functional is much higher and as a result these solutions become less important in the calculation of a minimum value of the functional. For a sufficiently high value of α, the spurious solutions are pushed quite far from the minimum variational solutions of the true solutions of the

waveguide so that they do not appear as real solutions. The effect of α, thus, is that of an easy implementation of the Coulomb gauge, $\nabla.\mathbf{H} = 0$. Thus, the presence of the spurious modes is greatly diminished.

For the slab waveguide case, we assume that the waveguide is infinite in x [Figure 2.1]. Thus,

$$J = SV \oint \left[(\nabla X \mathrm{H})^{*}.\hat{\varepsilon}_r^{-1}.(\nabla X \mathrm{H}) - k^2 \mathrm{H}^{*}.\hat{\mu}_r.\mathrm{H} + \alpha.(\nabla.\mathrm{H})^{*}.(\nabla.\mathrm{H}) \right] dy. \tag{3.1.11}$$

In the general, isotropic infinite waveguide case, the wave equations lead to

$$H_x = \frac{j\left(\omega\varepsilon \frac{\partial E_z}{\partial y}\right)}{(k^2 - \beta^2)} \tag{3.1.12}$$

$$H_y = -\frac{j\left(\beta \frac{\partial H_z}{\partial y}\right)}{(k^2 - \beta^2)} \tag{3.1.13}$$

$$E_x = -\frac{j\left(\omega\mu \frac{\partial H_z}{\partial y}\right)}{(k^2 - \beta^2)} \tag{3.1.14}$$

$$E_y = -\frac{j\beta\left(\frac{\partial E_z}{\partial y}\right)}{(k^2 - \beta^2)} \tag{3.1.15}$$

We can see that the transverse components H_X, H_Y, E_X and E_Y are purely real and the longitudinal components H_Z and E_Z can be taken as purely imaginary. This is common even in anisotropic waveguides and can be used for most problems [1]. This enables us to significantly reduce, by a factor of 2, the number of computational variables in the problem.

3.2 ELEMENTAL FORMULATION

We now discuss the creation of the problem for the individual elements. The problem as illustrated in Figure 2.1 is discretized as shown in Figure 3.2.1.

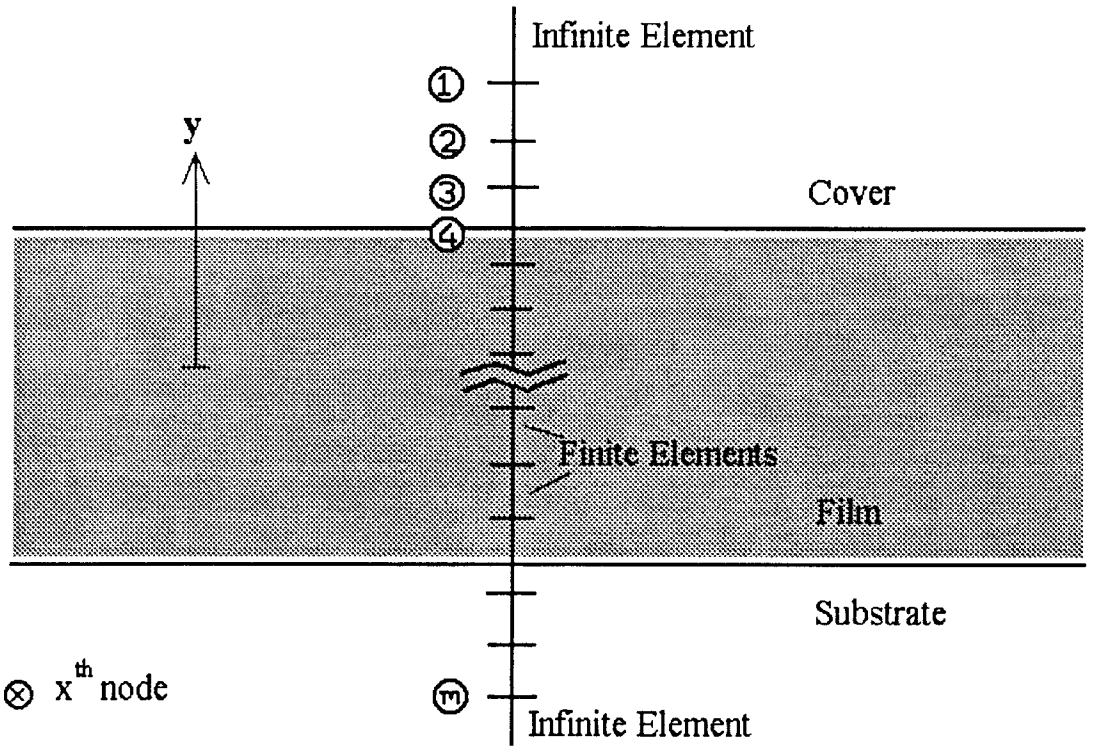

FIGURE 3.2.1 Creation of finite and infinite elements

The finite elements are along the y axis, as shown. By dividing the space with m nodes, we are creating m - 1 finite elements and 2 infinite elements extending to positive and negative infinity respectively, to describe the fields

sufficiently beyond the area of interest. The infinite elements are described in the next section.

3.2.1 Finite Elemental Formulation

We choose a first order linear interpolation of the fields in each finite element. In each element, the field at any point is represented, as shown in Figure 3.2.2, as

$$\mathbf{H}_{(y)} = L_1.\mathbf{H}_1 + L_2.\mathbf{H}_2 \tag{3.2.1}$$

where $$L_1 = \frac{y_2 - y}{y_2 - y_1} \tag{3.2.2}$$

and $$L_2 = \frac{y - y_1}{y_2 - y_1}, \tag{3.2.3}$$

so that $L_1 + L_2 = 1$ (3.2.4)

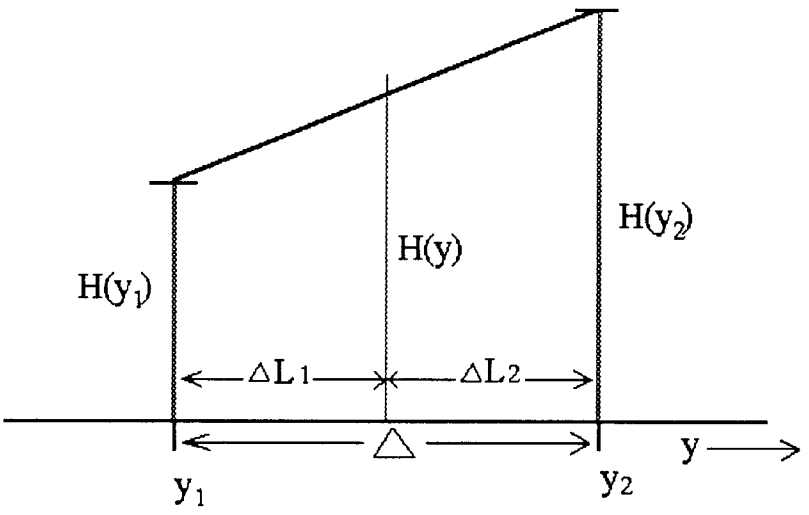

FIGURE 3.2.2 The Finite Element

We implement the formulation by using

$$\nabla = (0, \frac{\partial}{\partial y}, -j\beta), \tag{3.2.5}$$

and $$\nabla^* = (0, \frac{\partial}{\partial y}, j\beta). \tag{3.2.6}$$

Operating on

$$(\mathbf{H}) = [\hat{a}_x L_1 \quad \hat{a}_x L_2 \quad \hat{a}_y L_1 \quad \hat{a}_y L_2 \quad \hat{a}_z L_1 \quad \hat{a}_z L_2].[H_c], \text{ and} \tag{3.2.7}$$

$$(\mathbf{H})^* = [\hat{a}_x L_1 \quad \hat{a}_x L_2 \quad \hat{a}_y L_1 \quad \hat{a}_y L_2 \quad -\hat{a}_z L_1 \quad -\hat{a}_z L_2].[H_c]. \tag{3.2.8}$$

where

$$[H_c]^T = [H_{x1} \quad H_{x2} \quad H_{y1} \quad H_{y2} \quad H_{z1} \quad H_{z2}] \tag{3.2.9}$$

The subscripts 1 and 2 denote the nodes of the finite element.

This results in

$$(\nabla \times \mathbf{H})^* = [\ \hat{a}_y j\beta L_1 + \hat{a}_z/\Delta \quad \hat{a}_y j\beta L_2 - \hat{a}_z/\Delta \quad -\hat{a}_x j\beta L_1 \quad -\hat{a}_x j\beta L_2 \quad \hat{a}_x/\Delta \quad -\hat{a}_x/\Delta\ ].[H_c] \tag{3.2.10}$$

$$(\nabla \times \mathbf{H}) = [\ -\hat{a}_y j\beta L_1 + \hat{a}_z/\Delta \quad -\hat{a}_y j\beta L_2 - \hat{a}_z/\Delta \quad \hat{a}_x j\beta L_1 \quad \hat{a}_x j\beta L_2 \quad -\hat{a}_x/\Delta \quad \hat{a}_x/\Delta\ ].[H_c] \tag{3.2.11}$$

$$(\nabla \cdot \mathbf{H})^* = [0 \quad 0 \quad -1/\Delta \quad 1/\Delta \quad -j\beta L_1 \quad -j\beta L_2].[H_c] \tag{3.2.12}$$

$$(\nabla \cdot \mathbf{H}) = [0 \quad 0 \quad -1/\Delta \quad 1/\Delta \quad -j\beta L_1 \quad -j\beta L_2].[H_c] \tag{3.2.13}$$

where

$$\Delta = y_2 - y_1 \tag{3.2.14}$$

We can now write

$$\int_{y1}^{y2} \left[(\nabla X \mathrm{H})^* . \varepsilon_r^{-1} . (\nabla X \mathrm{H})\right] . dy = [H_c]^T . [\mathrm{M}] . [H_c] \tag{3.2.15}$$

$$\alpha . \int_{y1}^{y2} \left[(\nabla . H)^* . \mu_r . (\nabla . H)\right] . dy = [H_c]^T . [\mathrm{N}] . [H_c] \tag{3.2.16}$$

$$\int_{y1}^{y2} \left[(H)^* . (H)\right] . dy = [H_c]^T . [\mathrm{P}] . [H_c] \tag{3.2.17}$$

where M,N and P are scalar matrices that use the relationships

$$\int_{y1}^{y2} dy = \Delta \tag{3.2.18}$$

$$\int_{y1}^{y2} L_1 . dy = \int_{y1}^{y2} L_2 . dy = \frac{\Delta}{2} \tag{3.2.19}$$

$$\int_{y1}^{y2} L_1 . L_2 . dy = \frac{\Delta}{6} \tag{3.2.20}$$

$$\int_{y1}^{y2} L_1^2 . dy = \int_{y1}^{y2} L_2^2 . dy = \frac{\Delta}{3} \tag{3.2.21}$$

3.2.2 Infinite Elemental Formulation

The implementation of the variational formulation for the infinite elements is at a very large distance from the waveguide or area of interest where the fields are known to decay exponentially into the cladding. The infinite elements are shown in Figure 3.2.1. The fields in this area are taken as

$$\mathbf{H}(y) = \mathbf{H}(y_1).\exp[-(y-y_1)/L] \tag{3.2.22}$$

This field distribution is illustrated in figure 3.2.3.

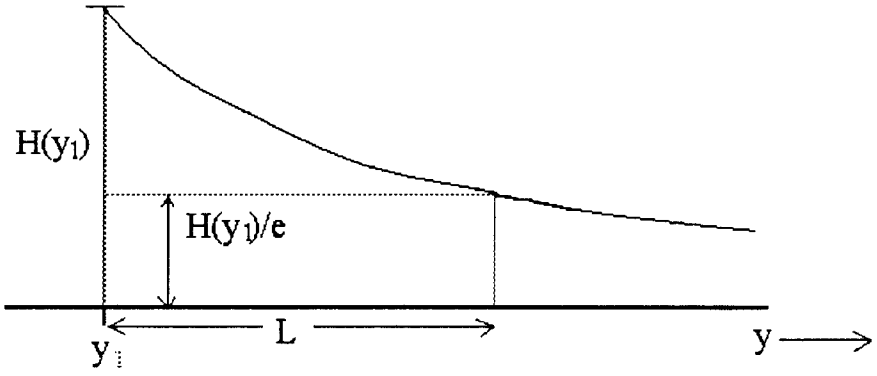

FIGURE 3.2.3 The Infinite Element

The choice of the decay length, L is not critical to the problem [16] when the infinite elements are chosen sufficiently distant from the dielectric interface where the contribution of the infinite elements to the variational formulation to the problem is relatively weak. As the decay length varies with the particular mode being considered, the implementation only needs to be a good approximation. This is achieved by using equations 3.2.5 and 3.2.6, which gives us

$$(\nabla \times \mathbf{H})^* = [\hat{a}_z.L + \hat{a}_y.j\beta \quad -\hat{a}_z.j\beta \quad \hat{a}_x.L].[H_c] \tag{3.2.23}$$

$$(\nabla \times \mathbf{H}) = [\hat{a}_z.L - \hat{a}_y.j\beta \quad \hat{a}_z.j\beta \quad -\hat{a}_x.L].[H_c] \tag{3.2.24}$$

$$(\nabla . \mathbf{H})^* = \left[0 \quad -\tfrac{1}{L} \quad -j\beta\right].[H_c] \tag{3.2.25}$$

and

$$(\nabla . \mathbf{H}) = \left[0 \quad -\tfrac{1}{L} \quad -j\beta\right].[H_c]. \tag{3.2.26}$$

Again, we can write

$$\int_{y1}^{y2} \left[(\nabla X \mathrm{H})^{*}.\varepsilon^{-1}.(\nabla X \mathrm{H})\right].dy = [H_c]^{T}.[\mathrm{M}].[H_c] \tag{3.2.27}$$

$$\alpha.\int_{y1}^{y2}\left[(\nabla.H)^{*}.\mu_r.(\nabla.H)\right].dy = [H_c]^{T}.[\mathrm{N}].[H_c] \tag{3.2.28}$$

$$\int_{y1}^{y2}\left[(H)^{*}.(H)\right].dy = [H_c]^{T}.[\mathrm{P}].[H_c] \tag{3.2.29}$$

where $$[H_c]^{T} = [H_{x1} \quad H_{y1} \quad H_{z1}] \tag{3.2.30}$$

The infinite element formulation above can be implemented at as many locations as required. An appropriate use of the exponential decay constant suitable to the position of implementation can be chosen.

3.3 LINKING OF ELEMENTS

In the previous section we have discussed the implementation of the variational formulation to each individual element of the discretized problem. We now discuss the mechanism of integrating the discretized implementation to include the entire problem.

The finite and infinite elements that form the problem share nodes with the other finite and infinite elements. We can achieve the complete problem description by explicitly describing these links. Using the linkage mechanisms, we can unite the formulations derived in the previous section.

We can unite the discretized problem by repositioning the elemental formulations. For a problem that has n total elements sharing m nodes, n = m+1, as illustrated in figure 3.2.1, the formulation in equation 3.1.11 can be stated as

$$J = SV\left[H_{dis}{}^{T}.X.H_{dis} - k^{2}.H_{dis}{}^{T}.Y.H_{dis}\right] \tag{3.3.1}$$

so that $$\left[H_{dis}\right]^{T} = \left[H_{c1}{}^{T} \quad H_{c2}{}^{T} \quad H_{c3}{}^{T} \quad .... \quad H_{cn}{}^{T}\right]^{T} \tag{3.3.2}$$

where $\left[H_{ci}\right]$ is the column H matrix that is associated with the i^{th} element and

$$\left[X\right] = \begin{bmatrix} M_1+N_1 & 0 & 0 & ..... & 0 \\ 0 & M_2+N_2 & & & 0 \\ . & & M_3+N_3 & & . \\ . & & & .... & . \\ 0 & 0 & 0 & ..... & M_n+N_n \end{bmatrix} \tag{3.3.3}$$

$$\left[Y\right] = \begin{bmatrix} P_1 & 0 & 0 & ..... & 0 \\ 0 & P_2 & & & 0 \\ 0 & & P_3 & & . \\ . & & & ..... & . \\ 0 & 0 & 0 & ..... & P_n \end{bmatrix} \tag{3.3.4}$$

We have

$$\left[H_{dis}\right] = \left[C\right].\left[H_{conn}\right] \tag{3.3.5}$$

$$\left[H_{conn}\right]^{T} = \left[H_{x1} \quad H_{y1} \quad H_{z1} \quad H_{x2} \quad H_{y2} \quad H_{z2} \quad ..... \quad H_{xm} \quad H_{ym} \quad H_{zm}\right]^{T}. \tag{3.3.6}$$

$\left[H_{conn}\right]$ is the column H - field array that describes the fields at the nodes of the connected problem. $\left[C\right]$ is the Connection Matrix whose elements take a value of 1 when the node of an element coincides with that of the connected problem and 0 otherwise.

We now have the new formulation matrices,

$$[H_{dis}]^T.[X].[H_{dis}] = [H_{conn}]^T.[A].[H_{conn}], \text{ and} \tag{3.3.7}$$

$$[H_{dis}]^T.[Y].[H_{dis}] = [H_{conn}]^T.[B].[H_{conn}], \tag{3.3.8}$$

i.e., $$[A] = [C]^T.[X].[C] \tag{3.3.9}$$

and $$[B] = [C]^T.[Y].[C] \tag{3.3.10}$$

Hence, equation 3.3.1 reduces to

$$J = SV\left[H_{conn}{}^T.A.H_{conn} - k^2.H_{conn}{}^T.B.H_{conn}\right] \tag{3.3.11}$$

The stationary nature of the functional is with respect to the variables in equation 3.3.11, i.e., the fields at the nodes of the problems. Thus, the variational function is minimized as

$$\frac{\partial J}{\partial H_i} = 0 \tag{3.3.12}$$

where H_i is an individual field component at any node. Since the field components at any node are independent variables, we can rewrite equation 3.3.12 as

$$[A].[H_{conn}] - k^2.[B].[H_{conn}] = 0 \tag{3.3.13}$$

Thus, the finite element problem is now an eigenvalue problem where the equation 3.3.13 is a formulation in terms of β. The eigenvalues give us the square of the wave numbers $k_i^2 = \left(\frac{2\pi}{\lambda_0}\right)^2$ that are supported by the waveguide at the given propagation constant β. The eigenvectors $[H_{conn}]_i$ give the

values of the H-field that correspond to the particular mode. As described in section 3.1.2, the components H_x and H_y are purely real and H_z is purely imaginary. The problem, once set up, can be solved repeatedly for different values of β to cover the range of interest.

Thus, knowing the way the problem has been discretized and by calculating the eigenvalues and eigenvectors of the variational formulation for a particular value of β, we can determine the values of the wave number, k, and the effective index, N_{eff}, that corresponds to the possible modes at that value of β.

3.4 ANALYSIS

3.4.1 Multimode waveguide

Figure 3.4.1 shows an asymmetric dielectric slab waveguide. The waveguide consists of 7000 Å of PECVD grown SiON of refractive index 1.8 that is deposited on a BK - 7 glass substrate of refractive index 1.52. The cover layer is air (n = 1).

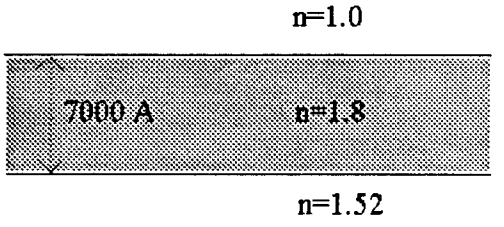

FIGURE 3.4.1 The Multimode Waveguide

The plots of β versus the effective index, N_{eff} are shown in figure 3.4.2 for the TE and TM modes. The dispersion curves (β versus k) are shown in figure 3.4.3 and the variation of the effective index, N_{eff} versus k is shown in figure 3.4.4. Due to the asymmetry of the problem, all the modes of the waveguide experience a cutoff at $k > 0$. A plot of the field distribution for the first 2 TE and TM modes at $k = 9.929 / \mu m$ (i.e., $\lambda_0 = 6328$ Å) are shown in figure 3.4.5.

3.4.2 Single mode waveguide

Figure 3.4.6 shows a different waveguide structure. The asymmetric single mode waveguide consists of a cover layer of air (n=1) and a substrate of glass (n=1.52) with the waveguide itself being a SiON layer 1620Å thick of refractive index 1.8.

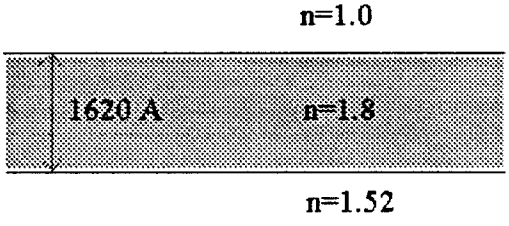

FIGURE 3.4.6 The Single Mode Waveguide

Single mode waveguide structures are very useful in integrated optics applications. Figure 3.4.7 shows the plots of β versus N_{eff} for the TE and TM modes. The dispersion curves are shown in figure 3.4.8 and the variation of the effective index, N_{eff} versus k is shown in figure 3.4.9. This waveguide structure is also asymmetric and shows a cutoff for values of $k > 0$.

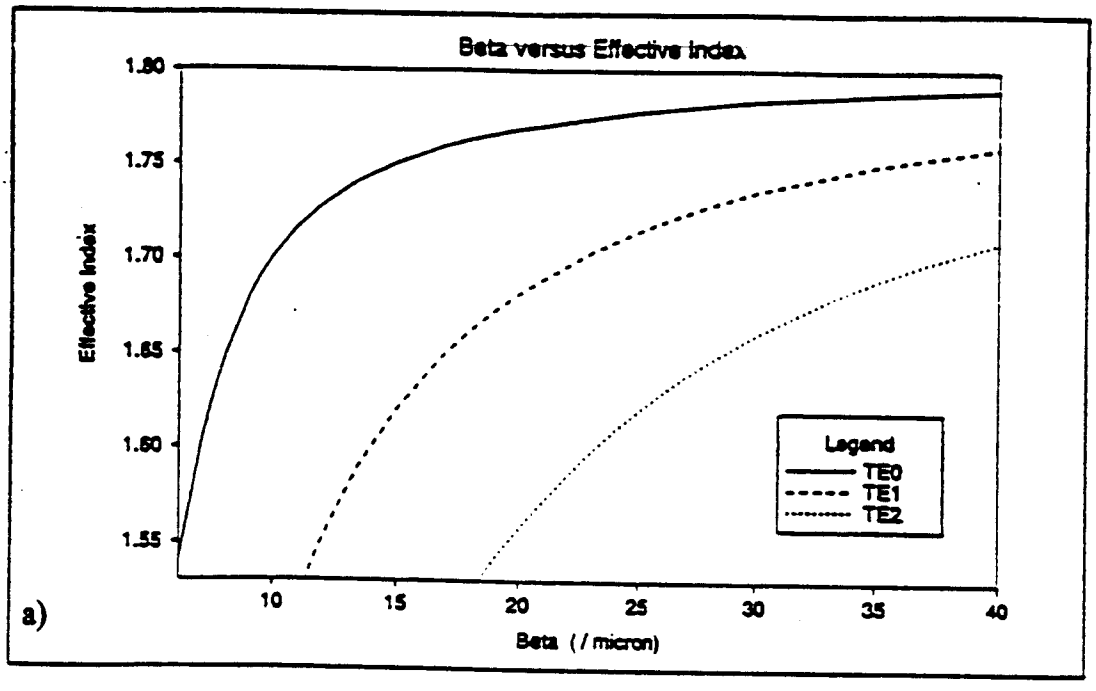

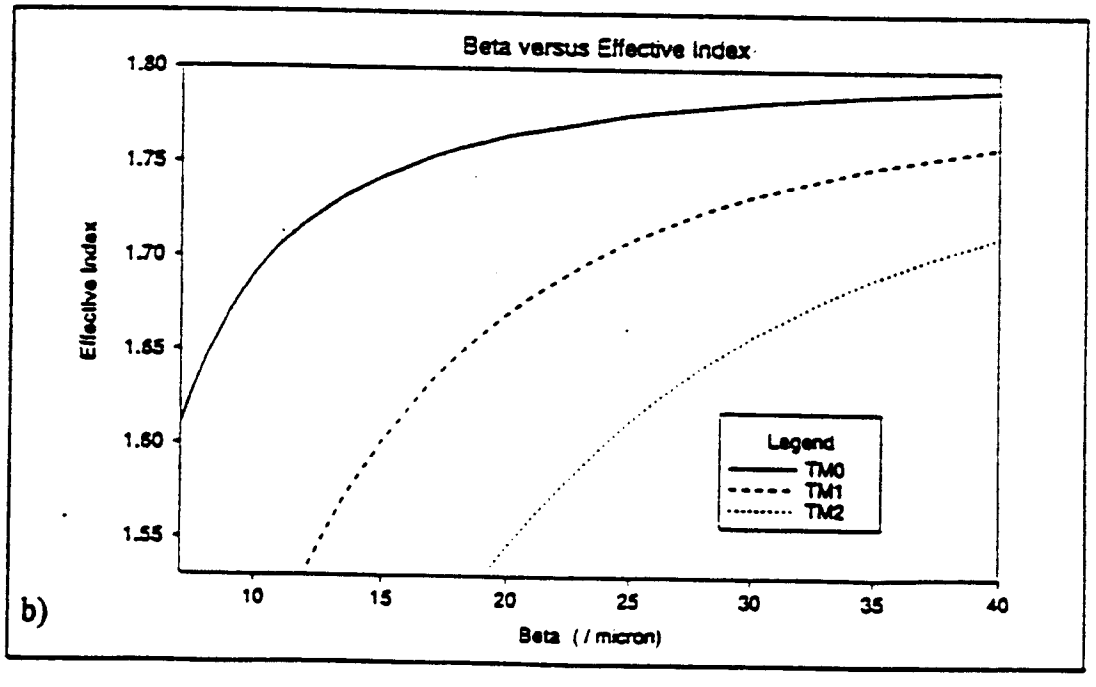

FIGURE 3.4.2 Beta versus Effective Index for the multimode waveguide

a) TE modes b) TM modes

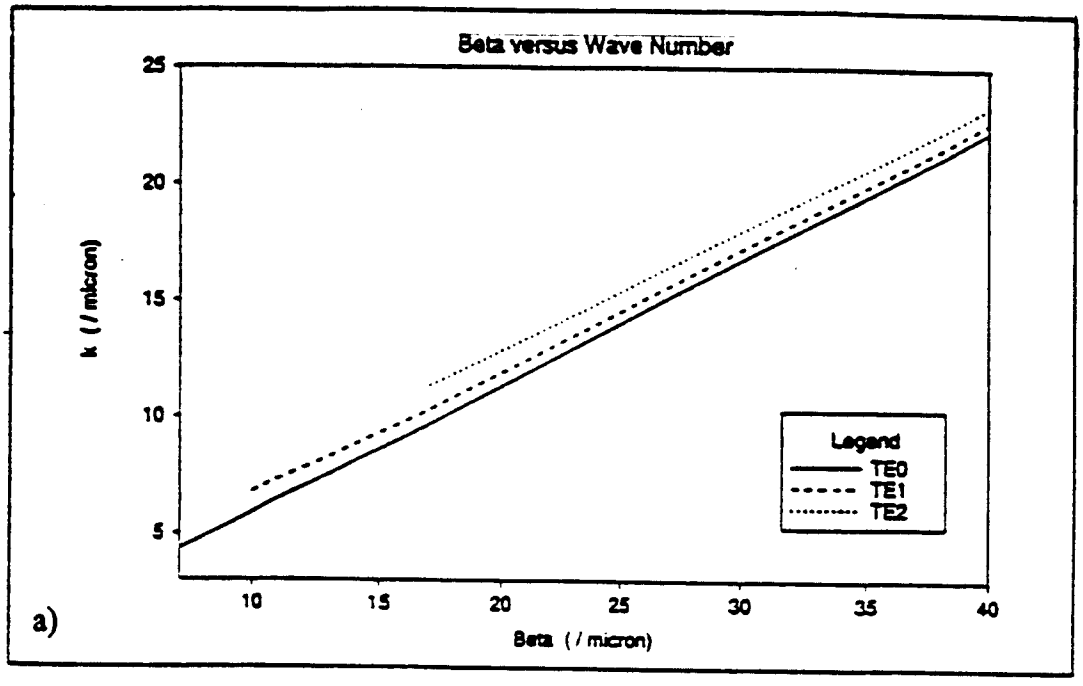

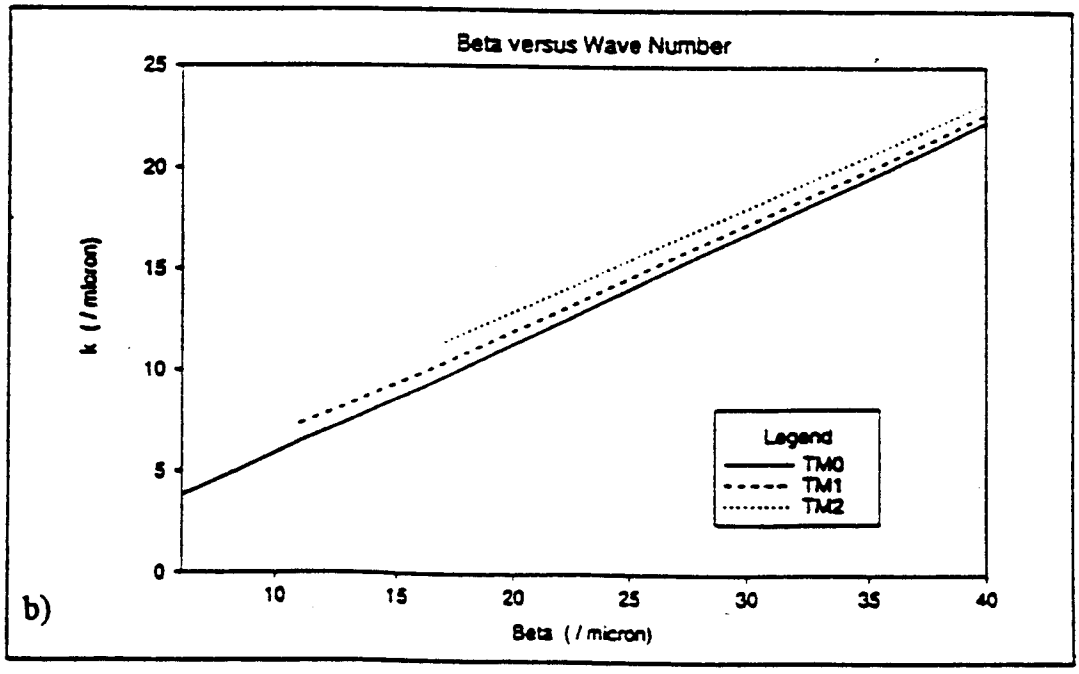

FIGURE 3.4.3 Beta versus Wave number for the multimode waveguide

a) TE modes b) TM modes

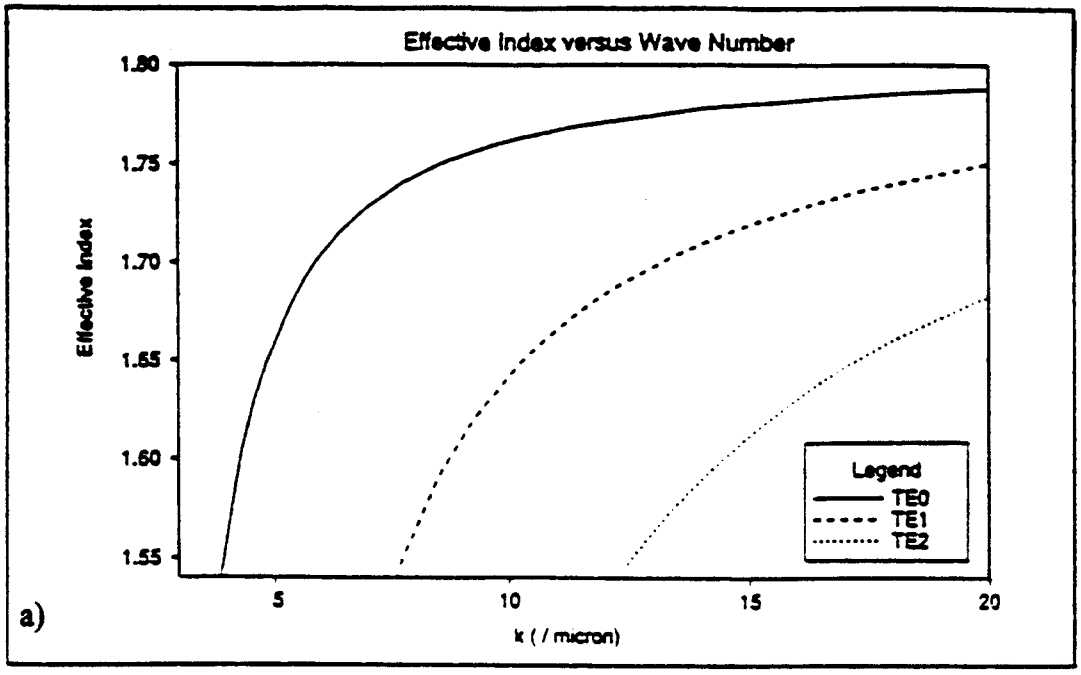

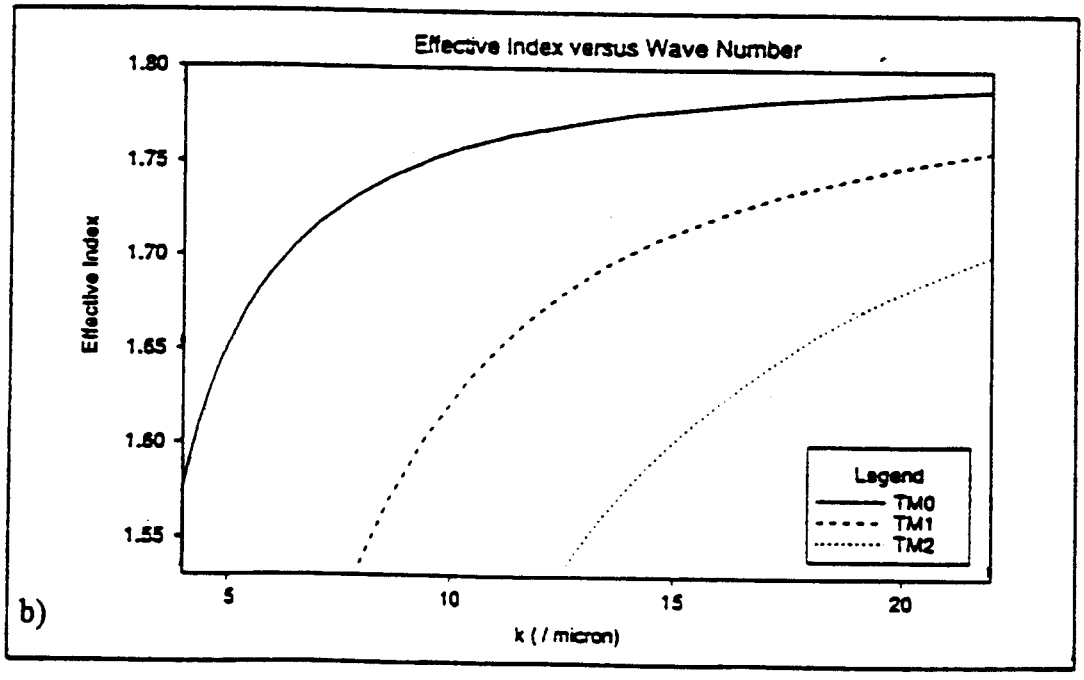

FIGURE 3.4.4 Effective index versus Wave number for the multimode waveguide

a) TE modes b) TM modes

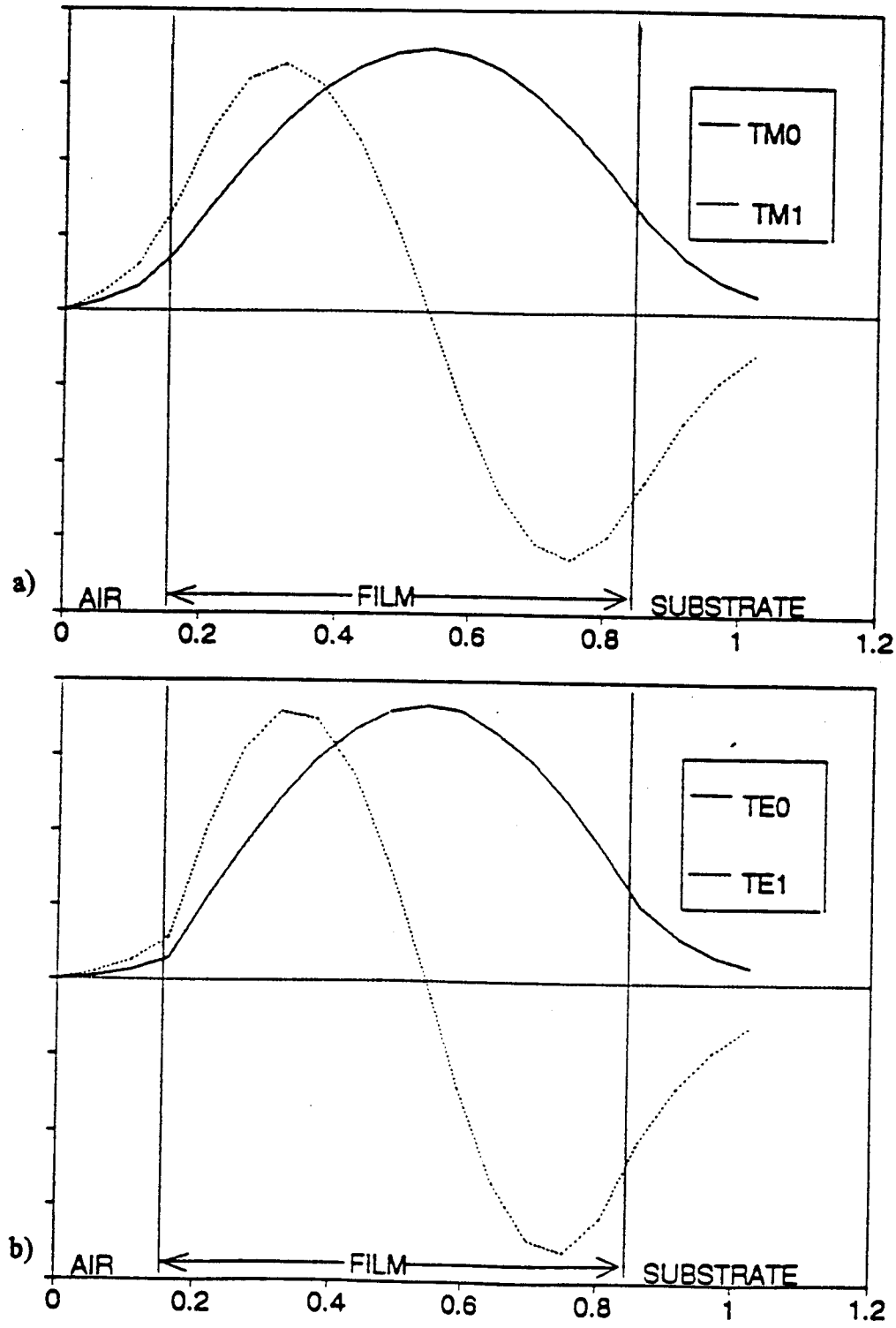

FIGURE 3.4.5 H - Field distribution in the multi mode waveguide at 632.8 nm

a) TM modes b) TE modes

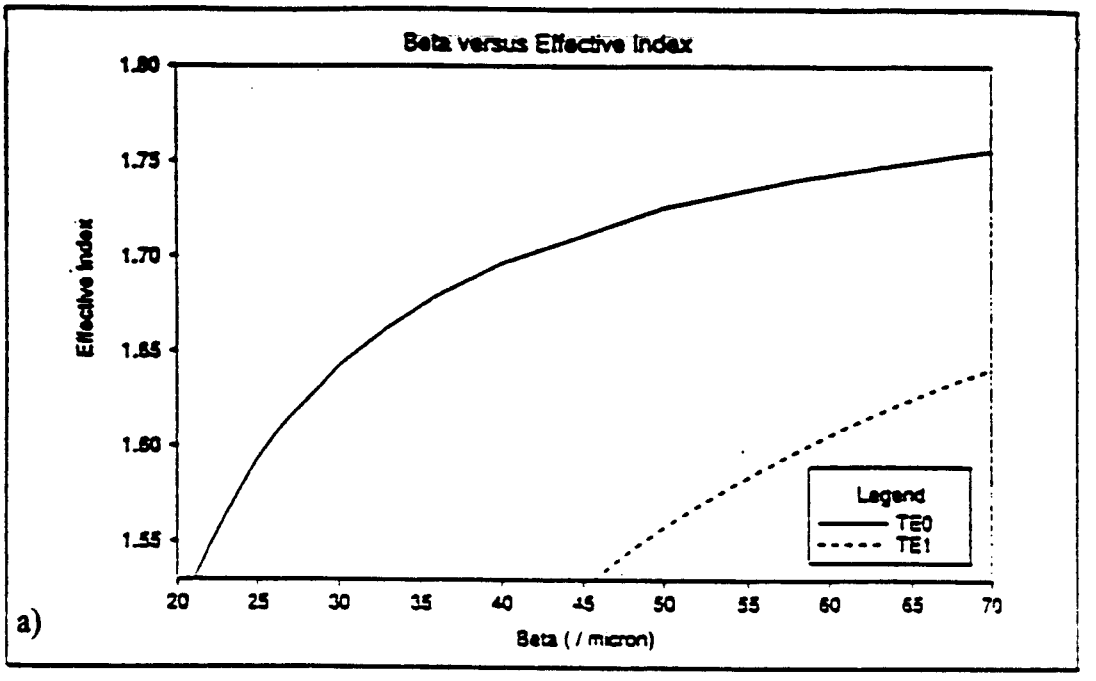

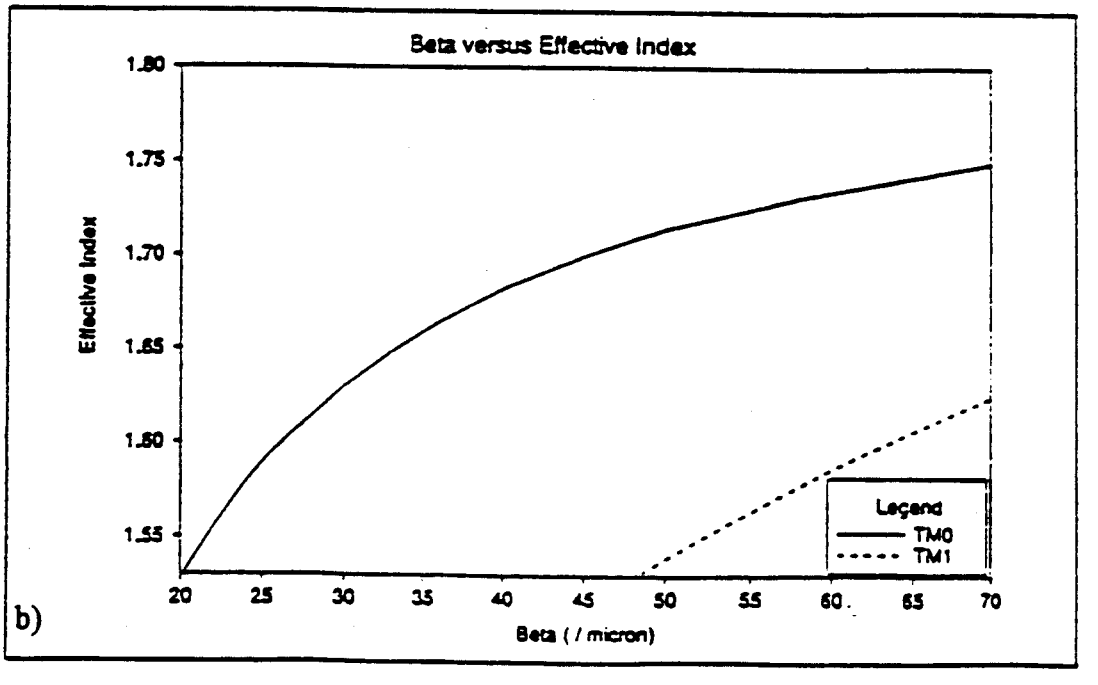

FIGURE 3.4.7 Beta versus Effective Index for the single mode waveguide

a) TE modes b) TM modes

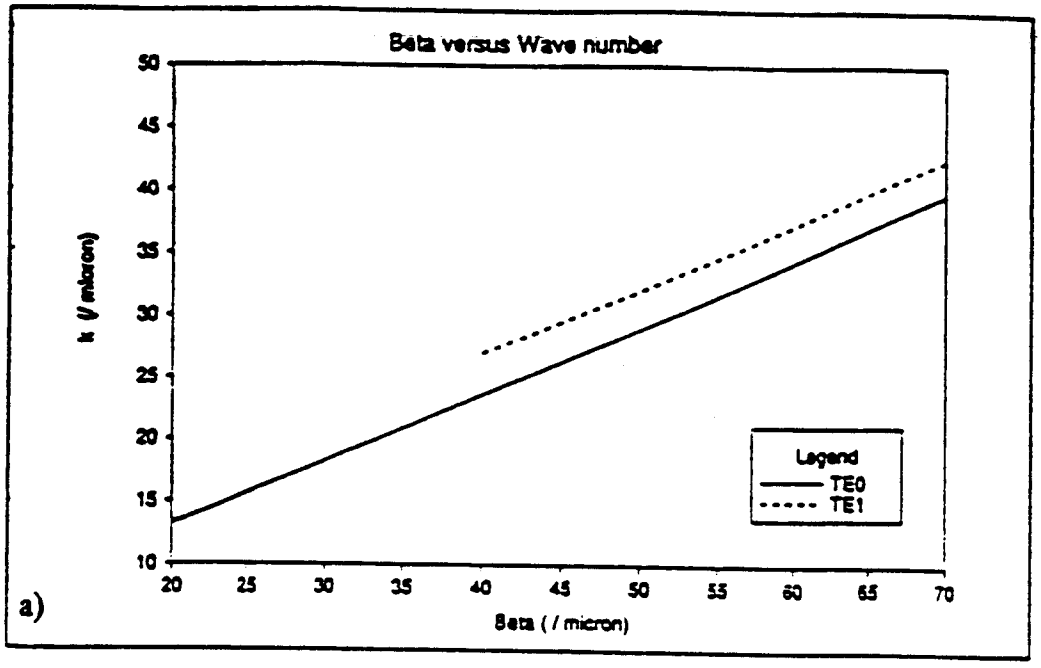

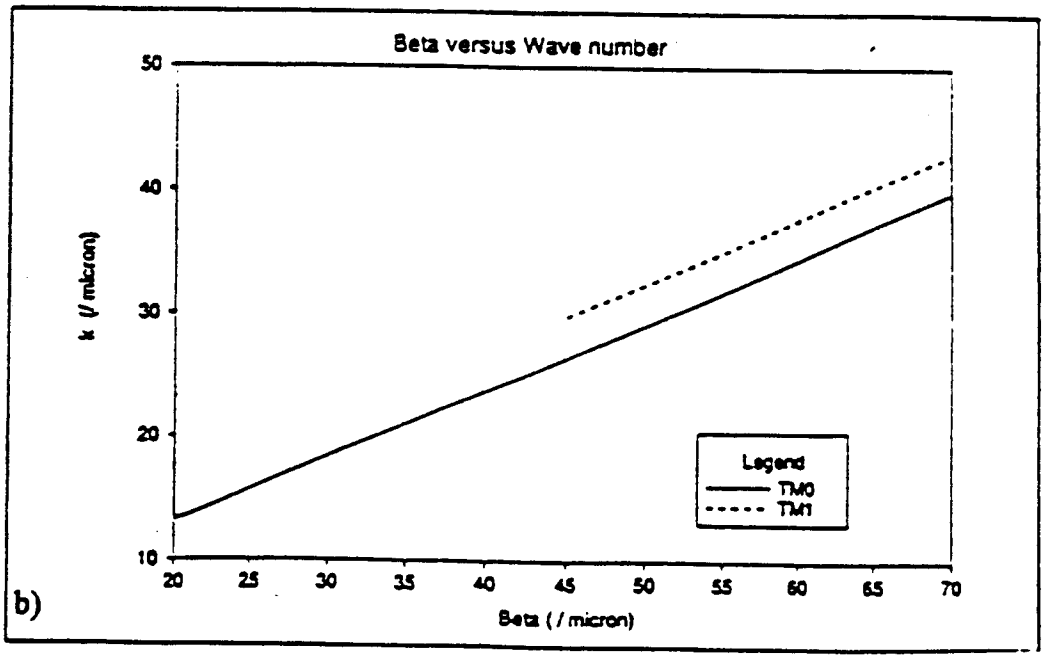

FIGURE 3.4.8 Beta versus Wave number for the single mode waveguide

a) TE modes b) TM modes

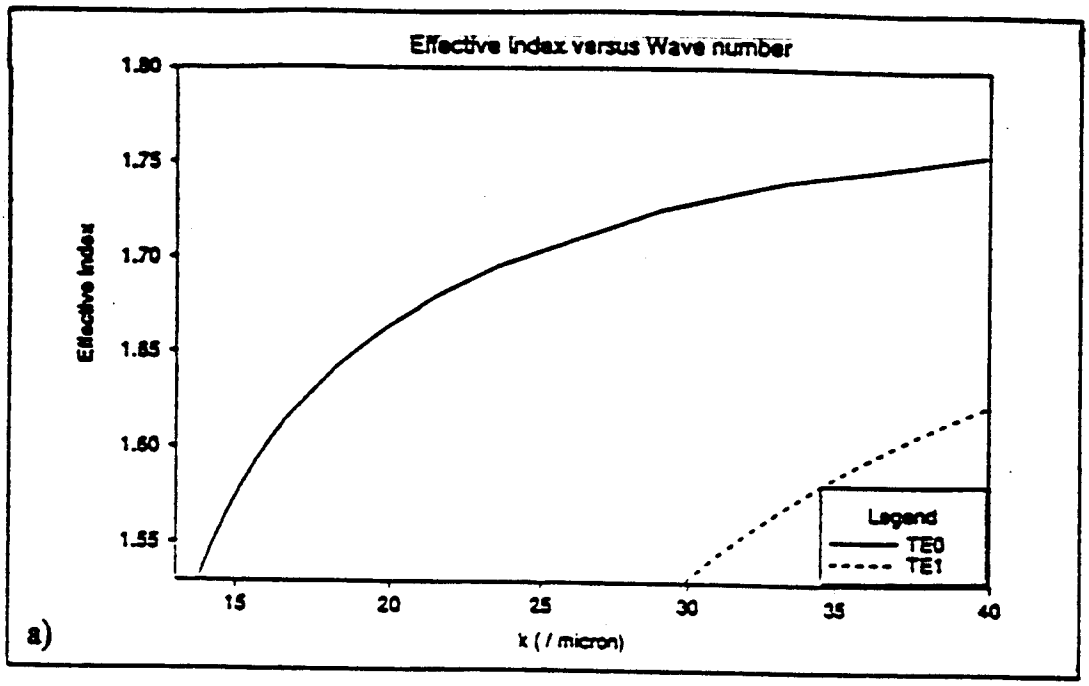

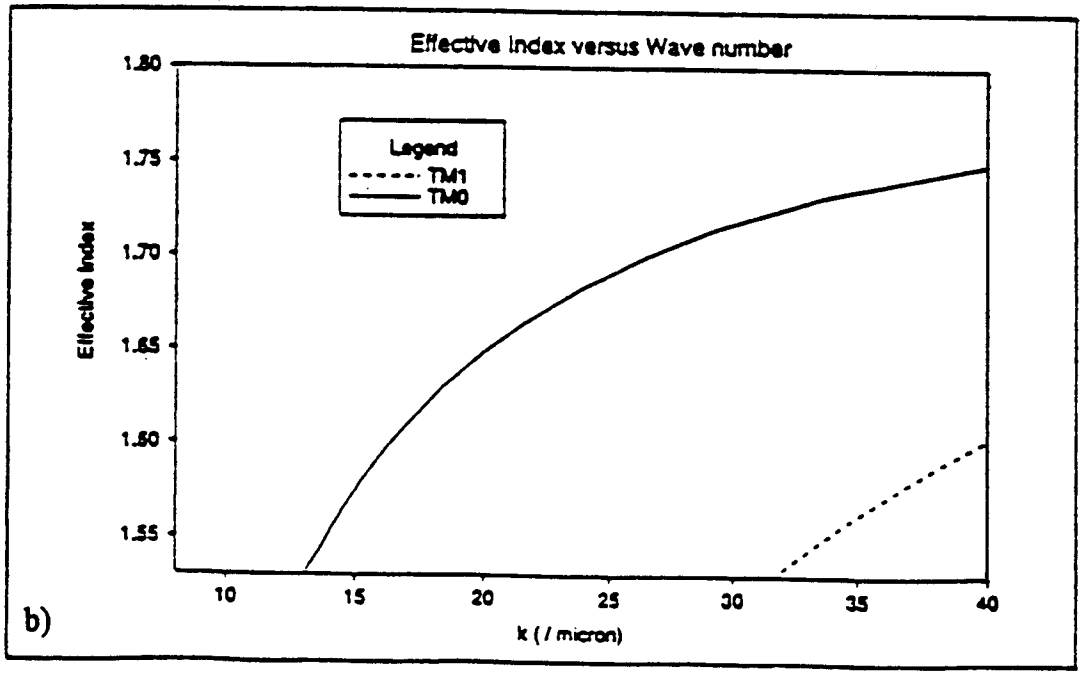

FIGURE 3.4.9 Effective Index versus Wave number for the single mode waveguide

a) TE modes b) TM modes

Analysis was also carried out for a single mode waveguide that consisted of a 3000 Å film of refractive index 1.8 with a superstrate of air and a substrate of glass (n = 1.52).

3.4.3 The Anisotropic Waveguide

Anisotropic waveguides are extremely important in integrated optics applications. A variety of anisotropic materials are used such as lithium niobate and lithium titanate [19,20]. Figure 3.4.10 illustrates a symmetric anisotropic waveguide. These values of the permittivity tensor were chosen to enable the comparison of results by the finite element method with those already documented [18].

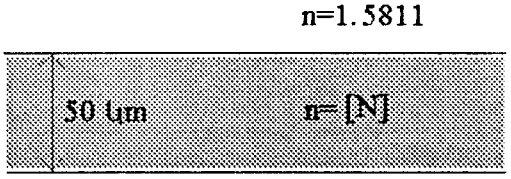

$$[N]=\begin{bmatrix} 2.287 & 0 & 0 \\ 0 & 2.2 & 0 \\ 0 & 0 & 2.287 \end{bmatrix}$$

FIGURE 3.4.10 The Anisotropic Waveguide

The waveguide has a permittivity tensor given by $\varepsilon_r = \begin{bmatrix} 5.23 & 0 & 0 \\ 0 & 4.84 & 0 \\ 0 & 0 & 5.23 \end{bmatrix}$.

The refractive index tensor can be calculated by remembering that $n_{ij} = \sqrt{\varepsilon_{ij}}$. The

cover and substrate layers are isotropic with refractive index 1.581 each. The TE modes are expected to show a higher effective refractive index due to the anisotropy of the problem. The modal dispersion curves for the TE and TM modes are shown in figure 3.4.11. The plots of the distribution of the H-field at $k = 9.929 / \mu m$ ($\lambda_0 = 6328$ Å) for the lower order TE and TM modes are shown in Figure 3.4.12.

The discussion of the results of the finite element simulations with experiment and other literature models is found in Chapter 5.

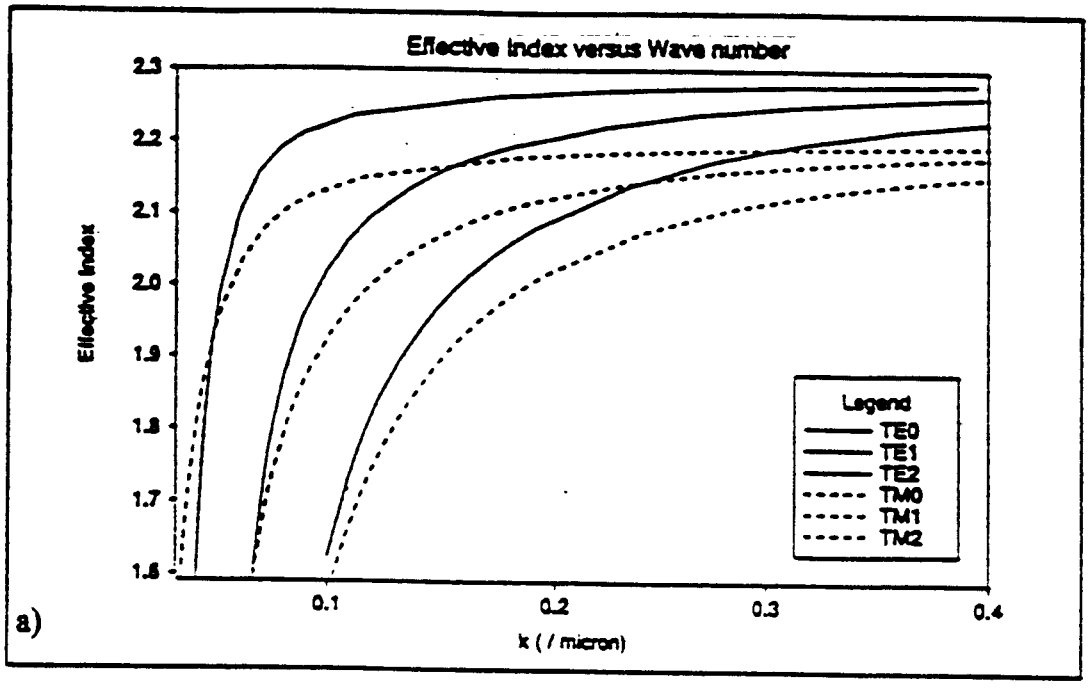

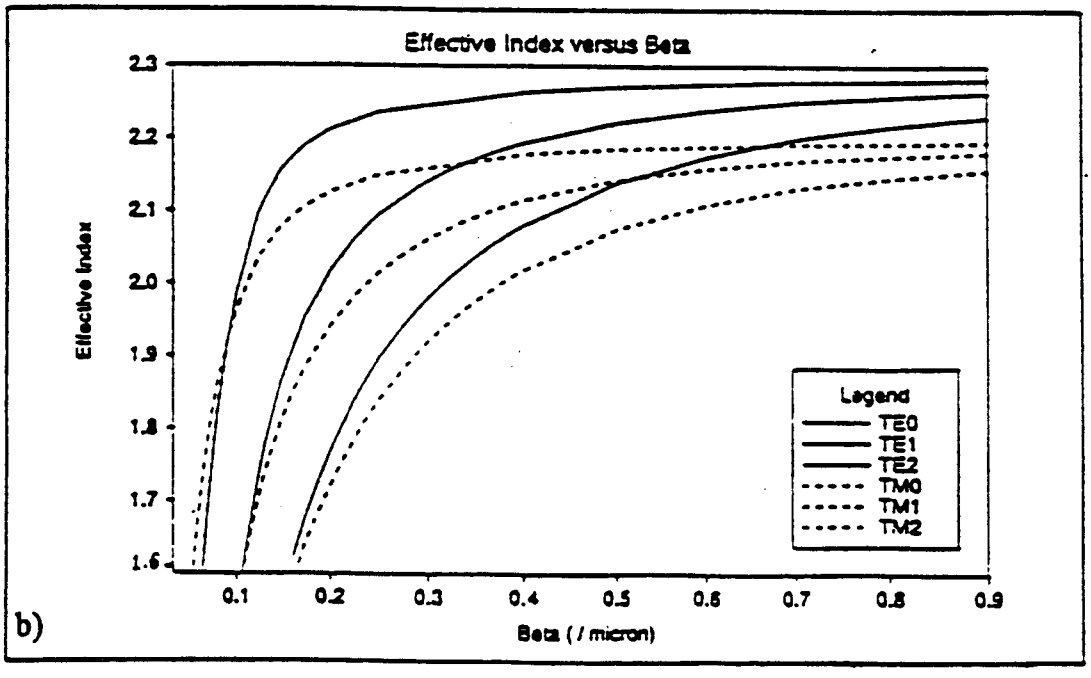

FIGURE 3.4.11 Effective Index versus a) Wave number and b) Beta for the anisotropic waveguide

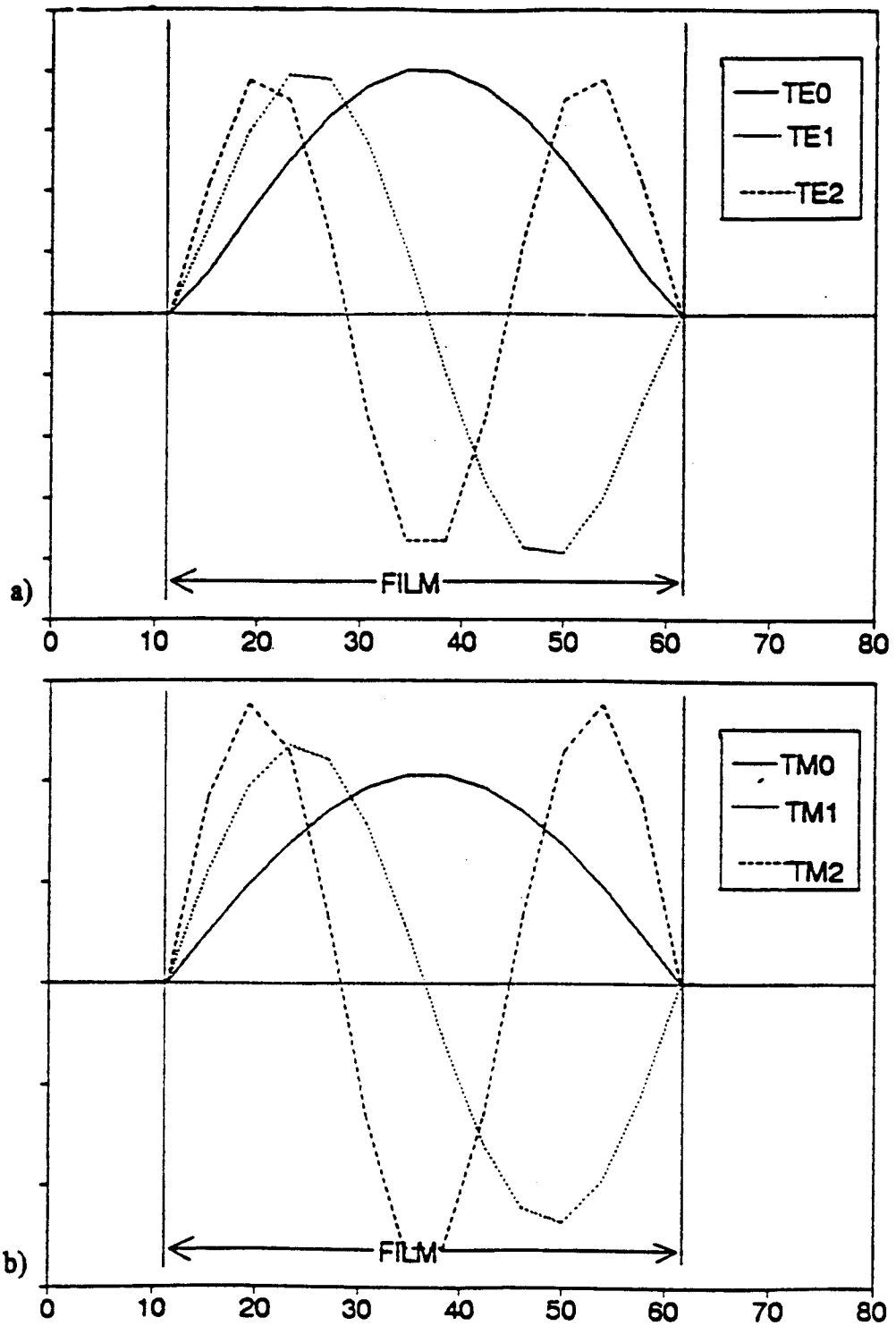

FIGURE 3.4.12 H - Field distribution in the anisotropic waveguide at 632.8 nm

a) TE modes b) TM modes

4. EXPERIMENTS

In order to experimentally verify the finite element model results, several single- and multimode slab waveguides were fabricated and measured. This chapter describes the processes used for waveguide fabrication, light coupling and effective index determination.

4.1 THE PECVD PROCESS

The waveguides were grown by depositing silicon oxynitride (SiON) films on 2" x 2" BK-7 glass substrates. The SiO_xN_y layers were deposited by the plasma enhanced chemical vapor deposition (PECVD) process. PECVD allows the growth of high quality films at low temperatures and at high deposition rates. In PECVD, the activation energy for the reactions is provided by an RF power source in the chamber. The set up of the growth process is shown in Figure 4.1.1. The gaseous reactants used were silane (SiH_4), nitrogen (N_2) and nitrous oxide (N_2O). The reactions occurring in the RF plasma are

$$SiH_4 + N_2O \xrightarrow{Plasma} SiO_x + H_2O$$

and

$$SiH_4 + N_2 \xrightarrow{Plasma} SiN_y + H_2.$$

The resultant deposition is thus a mixture of SiN_y:H and SiO_x:H which is amorphous in nature. The deposited film is best denoted by SiO_xN_y:H. The silane used was a 2% mixture in helium. The flow rates of the gases were SiH_4/He at 20 sccm (standard cubic centimeters per minute), N_2 at 10 sccm and N_2O from 0 to 50 sccm. The composition of the film can be varied from approximately SiO_2(n = 1.48) to Si_3N_4 (n = 2.05) by controlling the rate of flow of N_2O. The films

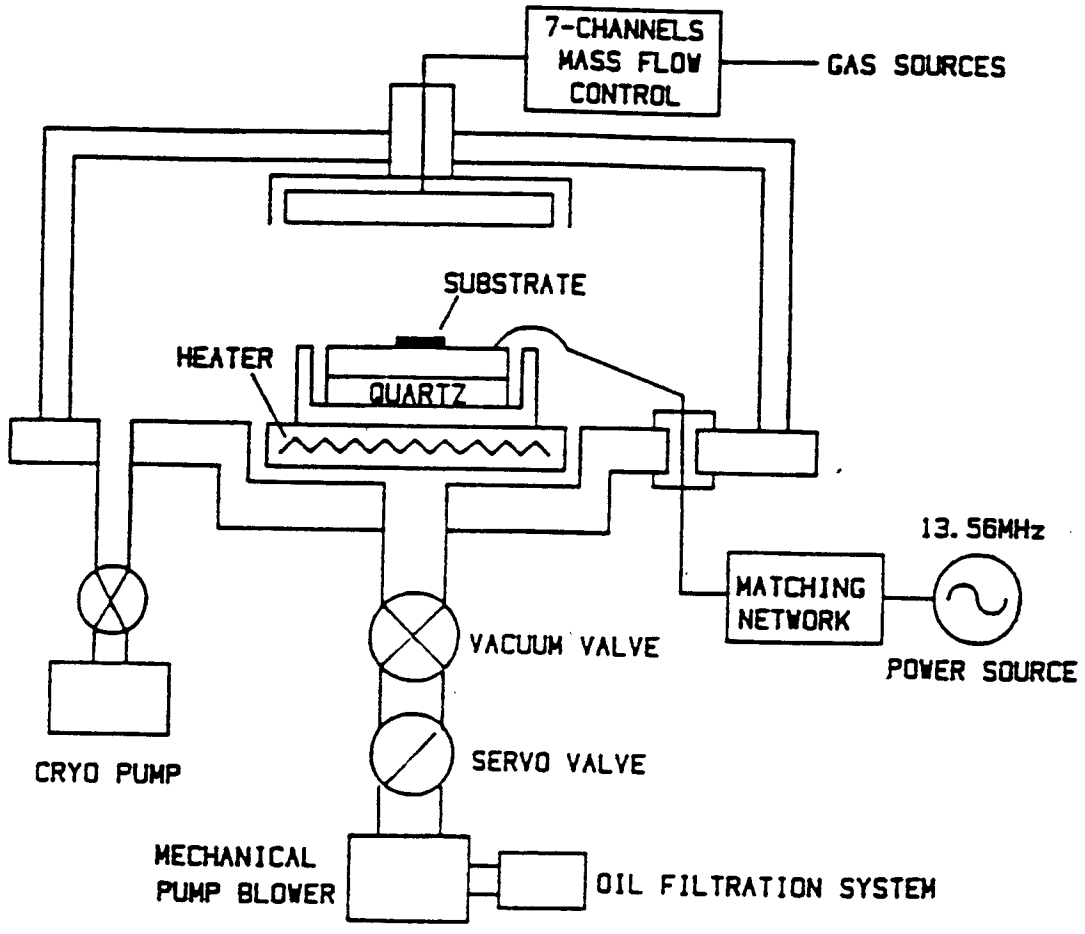

FIGURE 4.1.1 The PECVD film growth set up

deposited are actually SiO_X:H and SiN_y:H but the measured range of indices from 1.48 to 2.05 shows the limits to be nearly the same indices as the stoichiometric compounds. The substrate temperature was maintained at 300° C and the RF plasma provided was 70 Watts at 13.56 MHz. The deposition pressure in the plasma chamber was 500 mTorr.

The deposition rate has a strong dependence on the relative concentration of the reactants and on the RF power available in the chamber. The deposition rates ranged from 80 to 100 Angstroms per minute. The deposition process had been previously characterized with respect to the growth rate as a function of RF power and refractive index of the film as a function of the flow rate of N_2O, thus enabling the accurate control of refractive index and thickness of the layers.

Slight nonuniformities in the film thickness were noticed due to the nonuniformity of the substrate temperature across the area of the heated substrate. However, the variation across the central region of the substrate (roughly 2cm x 2cm) was not more than 5%.

The films grown were SiON films of refractive index 1.8, grown on BK-7 glass substrates of refractive index 1.52. The initial films grown had thicknesses of 1620Å for a weakly coupled single mode waveguide at 632.8 nm and 7000 Å for a multimode guide. Later, a 3000 Å thick single mode waveguide was grown for comparison and easier prism coupling.

4.2 WAVEGUIDE COUPLING

4.2.1 Experiment

To avoid problems in polishing and focusing for endfire coupling, the prism coupling technique was used to couple light into the waveguide structures. The

experimental set up is shown in Figure 4.2.1. A strontium titanate 45-45-90 prism was clamped down on the waveguide using a specially designed clamp stand. The waveguide along with the prism clamp was mounted on a rotational stage which was in turn mounted on an XYZ translation stage. The light source used was a 4mW HeNe laser operating at 632.8 nm with a TEM_{00} transverse mode. The strontium titanate prism has a refractive index of 2.38 at 632.8 nm. The beam was focused by a lens of focal length approximately 9 cm and aimed near the right angle corner of the prism. The angle at which the light was incident on the prism was controlled by the rotational stage. The XYZ translational stage was used to ensure that the light was incident at the right angle corner of the prism. A polarizer sheet was used to isolate the TE and the TM modes of the waveguide.

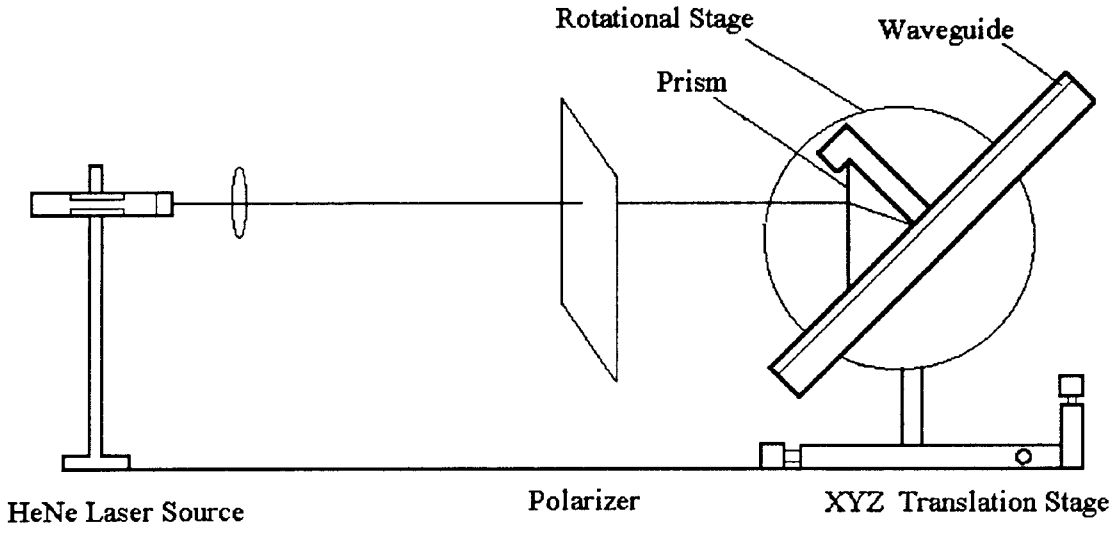

FIGURE 4.2.1 The Waveguide Coupling Set Up

The pressure with which the prism was clamped down over the waveguide was seen to have a significant effect on the coupling efficiency. For efficient coupling the prism-waveguide spacing must be small enough for the evanescent field to bridge the gap and couple to the waveguide. This requires spacings of less than a micron. It was also found that it was crucial that the light entered the waveguide exactly at the right angle corner of the prism. This ensured that the wave coupled into the waveguide could not immediately couple back into the prism and would continue to propagate down the waveguide.

4.2.2 Theory

The coupling action between the prism and the waveguide is illustrated in Figure 4.2.2.

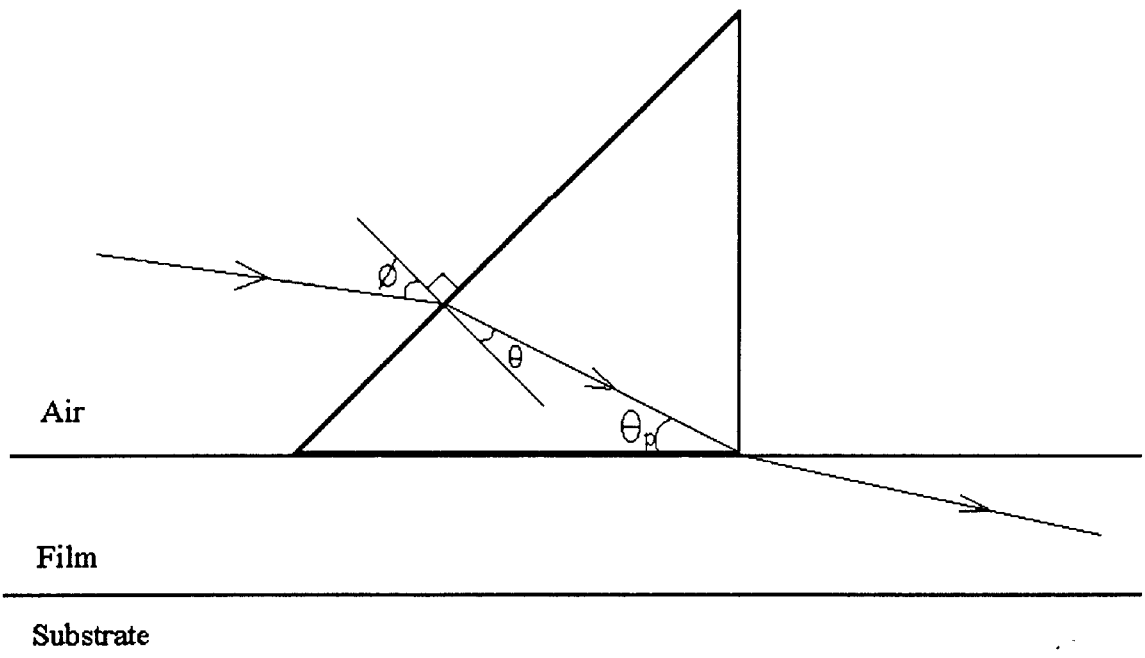

FIGURE 4.2.2 Prism Coupling into a waveguide

The light couples into the prism when the longitudinal component (parallel to the interface between the prism and the film) of the propagation constant of the light in the prism equals the longitudinal component of the propagation constant of the mode of the waveguide, providing the spacing is small enough to allow field coupling.

$$\beta_{prism} = \beta_{guide} \text{ , i.e.,}$$

$$\frac{2\pi}{\lambda_o} . n_p . \cos\theta_p = \beta_{guide}$$

where n_p is the refractive index of the prism.

By observing the angle to the normal of the prism, ϕ, at which light is coupled into the waveguide, we can calculate the longitudinal propagation constant in the waveguide, and thus, the effective index of the coupled mode.

5. RESULTS AND DISCUSSIONS

5.1 EXPERIMENTAL RESULTS

The waveguide structures that were fabricated were the ones described in sections 3.4.1 and 3.4.2. The multimode waveguide consisted of a 7000 Å thick SiON film of refractive index 1.8 deposited on a 0.040" thick glass substrate of refractive index 1.52. The single mode waveguides consisted of 1620 Å and 3000 Å thick films of refractive index 1.8 on BK-7 glass. In all the cases, the cover layer was air (n_c = 1.0).

HeNe light at 632.8 nm was successfully prism coupled into the waveguide structures. The waveguides were simulated by the finite element as well as by the direct matching method program [22]. For the HeNe wavelength, the free space wave number k_0 = 9.929 / μm. We can use this value of k_0 to determine the values of the propagation constant β and effective index N_{eff} predicted by the finite element program from Figures (3.4.3 and 3.4.4) and (3.4.8 and 3.4.9) for the multimode and the single mode cases, respectively. The comparison can now be made between the results of the direct matching method, the finite element method, and the experimental results. The values for the multimode case are tabulated in Table 5.1. The values for the single mode case of film thickness 1620 Å are shown in Table 5.2 and those for the single mode case of film thickness 3000 Å are shown in Table 5.3. For the experimentally observed values of the effective index, the error bars indicate the error present due to the least count of the rotational stage (about 0.5°) and the error inherent in the variations in film thickness (about 5 %).

Mode	Experimentally observed effective index	Exact Effective Index (Calculated from Direct Matching Method)	Effective Index (Calculated by Finite Element Method)
TE0	1.78 ± 0.007	1.7633	1.760
TE1	1.64 ± 0.007	1.6528	1.643
TM0	1.78 ± 0.007	1.7561	1.759
TM1	1.63 ± 0.007	1.6275	1.640

Comparison of experimental and predicted values of effective index for multi-mode case

TABLE 5.1

Mode	Experimentally observed effective index	Exact Effective Index (Calculated from Direct Matching Method)	Effective Index (Calculated by Finite Element Method)
TE0	1.59 ± 0.006	1.574	1.545

Comparison of experimental and predicted values of effective index for single mode case (film thickness 1620Å)

TABLE 5.2

Mode	Experimentally observed effective index	Exact Effective Index (Calculated from Direct Matching Method)	Effective Index (Calculated by Finite Element Method)
TE0	1.68 ± 0.006	1.6773	1.657
TM0	1.64 ± 0.006	1.6356	1.634

Comparison of experimental and predicted values of effective index for single mode case (film thickness 3000Å)

TABLE 5.3

5.2 DISCUSSIONS

5.2.1 Multimode waveguide case

In the case of the waveguide discussed in 3.4.1, which consisted of a 7000Å thick film of refractive index 1.8 deposited on a glass substrate of refractive index 1.52, by comparing the results obtained by the finite element method and the direct matching method, we see that the values are in quite close agreement. There is also good agreement with the experimentally measured values of the effective indices of the coupled modes. In repeated simulations using different values of decay lengths for the fields in the wings, it was also observed that the value of the decay length itself is not crucial to the accuracy of the result. In this case, all the modes are very well confined (N_{eff} is much closer to 1.8 than 1.52). This means that the strength of the fields in the cladding is very weak and so the variational

formulation in the infinite elements has very little effect on the total formulation of the problem. Thus, an inaccurate value of the decay length chosen will not adversely affect the final result. This is important to understand as the actual value of the decay length is different for each of the modes. The calculations have to be repeated to obtain accurate results for the various modes, where the result is only accurate for the mode being studied. This results in a large increase in the required computation time required to come to an accurate solution.

The value of the decay length can also be programmed as a variational parameter in the finite element problem formulation [16], so that the eigen solution gives us a value of the decay length. However, as observed earlier, this value should be different for each of the modes, so the resultant value is not "true" for any of the modes and is thus a poor approximation to all of them. Hence, this method was avoided.

The field distributions shown in figures 3.4.7 and 3.4.11 also show how the modes are more tightly confined at the film - air interface due to the large differential in refractive index at this interface. As the waveguide is asymmetric, i.e., $n_c \neq n_s$, the waveguide experiences a cutoff at $k_0 > 0$. The asymmetry of the waveguide permits $\beta \geq 0$ only for $k_0 > 0$ [1,2].

5.2.2 Single mode waveguide case

For the case of the 1620 Å thick film of refractive index 1.8 deposited on glass of refractive index 1.52, the calculations by the direct matching method [22] show the presence of just 1 mode (TE mode) with N_{eff} of 1.574. In other words, these modes are very poorly confined and the decay lengths of the fields in the wings is quite large. The initial calculated effective index of the mode, using the finite element program, was 1.504.

The match between the results of the direct matching method and those predicted by the finite element method show a greater error in this case. The values predicted by the finite element program differed by 5 %. The assumption that the waveguides are lossless is less accurate due to the poor confinement of the fields in the waveguide. In poorly confined modes, i.e., when the value of N_{eff} is very close to 1.52 (the substrate refractive index), the fields in the wings are higher and the variational functional is strongly dependent on an accurate value of the decay length chosen in the cladding. A good estimate of the values of the decay lengths to be used can be obtained by extending the finite element formulation deep into the cladding where the field decay can be observed. The decay rate observed in the cladding can now be used as a starting approximation to be used in the infinite elements. This procedure can be used iteratively in the infinite element formulation to give a better approximation of the actual decay length. This procedure yielded an effective index of 1.545 for the lowest order TE mode. This result is still quite different from the predictions of the direct matching method. The finite element problem is set up assuming the lossless propagation of the modes in the waveguide. This assumption is less valid in poor confinements that occur at low values of β. Hence, we observe greater errors in the predictions of the finite element method for modes that are close to cutoff.

To observe the improvement in accuracy of the predictions of the finite element method, another single mode waveguide was grown. In the case of the single mode film of thickness 3000 Å, as seen in Table 5.3, the experimental results and those of the finite element method and the direct matching method all show close agreement. Due to the greater confinement demonstrated in this case, the variational formulation is strongly dependent on the field distributions in the waveguide itself. The results of the simulations thus display a greater accuracy for well-confined modes.

We studied the effect of variation in assumed decay length in the cladding on the predicted effective index by the finite element method. Tables 5.3a and 5.3b show the variation of effective index for different chosen values of the decay length in the air and substrate layers of the single mode waveguide of film thickness 3000 Å. We observe that the variation in the predicted effective index is by as much as 1.5 % for minute variations in the decay lengths in the cladding.

FIELD DECAY LENGTH IN THE SUBSTRATE	EFFECTIVE INDEX (@ 632.8 nm)
0.1	1.65
0.12	1.656
0.14	1.657
0.16	1.657
0.18	1.657
0.2	1.655
0.22	1.655
0.24	1.654

TABLE 5.4 a

FIELD DECAY LENGTH IN AIR	EFFECTIVE INDEX (@632.8 nm)
0.01	1.65
0.014	1.652
0.018	1.653
0.022	1.655
0.025	1.657
0.028	1.657

TABLE 5.4 b

TABLE 5.4 Variation of effective index versus assumed field decay length in the cladding

5.2.3 Anisotropic Waveguide Case

The scalar permittivity used in the isotropic cases is replaced by a tensor permittivity to create the anisotropic case. Yamamoto, et.al. [18] have used a Rayleigh-Ritz variational method to obtain the dispersion curves for a lithium niobate film. The results of the simulations of the anisotropic case are shown in Figure 3.4.11. Table 5.5 gives a comparison of the predictions of the finite element program with those documented by Yamamoto et al, at a normalized thickness (d / λ_0) of 2.0. We observe a close agreement with the previously published results.

Mode	Effective Index (Calculated by Finite Element Method)	Effective Index (Predicted by Yamamoto et al)
TE0	2.286	2.286
TE1	2.235	2.231
TE2	2.154	2.17
TM0	2.188	2.189
TM1	2.154	2.15
TM2	2.086	2.083

Comparison of predicted values of effective index for anisotropic waveguide case

TABLE 5.5

The anisotropy results in the sharp difference in the maximum values of the effective indices of the TE and the TM modes as the electric fields are oriented along different principal axes for the 2 cases. This affects only the well-confined cases. For a poorly confined mode, there is not a great difference in the effective indices of the TE and the TM modes since a large portion of the wave exists in the wings making the effective index more dependent on the index of the cladding. Since PECVD produces amorphous waveguides, we were unable to experimentally prepare anisotropic waveguides to measure. Diffused waveguides in $LiNbO_3$ would provide anisotropic samples and could be pursued in the future.

5.3 CONCLUSIONS

The finite element method has been shown to be a useful tool in the prediction of dielectric waveguide characteristics. The details of the finite element program and its operating characteristics are given in Appendix 1. The advantages of using the finite element method in the study of integrated optical waveguides are in unconventional structures, asymmetries or anisotropies where analytical techniques fail, making it a very versatile tool to the integrated optics designer. The method has a high accuracy and allows an arbitrarily small discretization of the problem with comparatively small investment in memory and computation time which gives results of high accuracy.

The accuracy with which the results of the finite element method have matched experimental results and other previously documented results proves that the method is reliable. The modular nature of the programming allows for increasing the scope of the problem greatly in terms of accuracy and complexity without vastly increasing the complexity of the problem definition.

The method is quite accurate in dealing with well-confined modes in dielectric waveguides. However, when dealing with poorly confined modes (i.e., modes near cutoff) the method proves to be more inaccurate. The finite element solutions for poorly confined modes are very dependent on the assumed value of the exponential decay length in the cladding.

5.4 FUTURE WORK

An interesting application of the finite element analysis of dielectric waveguides that bears exploration is the study of two - dimensional and buried waveguide structures. To study the field distributions, phase interactions and power transmission between dielectric waveguides placed in proximity is another application. Such problems are of interest in the design of directional couplers, modulators and other common integrated optic structures. The finite element method is also well suited to the study of diffused waveguides where the film layers actually possess a complementary error function or other complicated distribution of refractive index. The fabrication of such structures to verify the simulations should be a simple task given the fabrication resources available.

REFERENCES

[1] P. Silvester and R.L. Ferrari, Finite Elements for Electrical Engineers, Cambridge University Press, Cambridge, 1990.

[2] D. Marcuse, Theory of Dielectric Optical Waveguides, 2nd ed., Academic Press, Boston, 1991.

[3] A.H. Cherin, An Introduction to Optical Fibers, McGraw Hill, New York, 1983.

[4] T. Itoh, Numerical Techniques For microwave And millimeter-wave Passive Structures, Wiley, New York, 1989.

[5] P. Silvester, "A General High-Order Finite Element Waveguide Analysis Program", IEEE Trans Microwave Theory Tech, vol. MTT-17, pp.204 - 209, April 1969.

[6] C.G. Williams and G.K.Campbell, "Numerical Solutions of Surface Waveguide Modes Using Transverse Field Components", IEEE Trans Microwave Theory Tech, vol. MTT-2, pp.329-332, March 1974.

[7] A.D. Berk, "Variational Principles for Electromagnetic Resonators and Waveguides", IRE Trans Antennas Propagat, vol AP-4, pp. 104-111, April 1956.

[8] M. Ikeuchi, H. Sawami and H. Niki, "Analysis of Open-Type Dielectric Waveguides by the Finite Element Iterative Method", IEEE Trans Microwave Theory Trans, vol. MTT-29, pp. 234-239, March 1981.

[9] P. Silvester and M.V.K. Chari, Finite Elements for Electrical Engineers, Wiley, Chichester, 1980.

[10] A. Konrad, "Vector Variational Formulation of Electromagnetic Fields in Anisotropic Media", IEEE Trans Microwave Theory Trans, vol. MTT-24, pp. 553-559, September 1976.

[11] I. Bardi and O. Biro, "An Efficient Finite Element Formulation Without Spurious Modes for Anisotropic Waveguides", IEEE Trans Microwave Theory Tech, vol 39, no. 7, pp. 1133-1138, July 1991.

[12] J.A. Svedin, "A Modified Finite Element Method for Dielectric Waveguides Using an Asymptotically Correct Approximation on Infinite Elements", IEEE Trans Microwave Theory Tech, vol. 39, no. 2, pp. 258-266, Feb. 1991.

[13] K. Bathe, Finite Element Procedures in Engineering Analysis, Prentice Hall, Englewood Cliffs, NJ, 1982.

[14] O.C. Zienkiewicz, The Finite Element Method, 3rd ed., McGraw Hill, 1977.

[15] N. Mabaya, P.E. Lagasse and P. Vandenbulcke, "Finite Element Analysis of Optical Waveguides", IEEE Trans Microwave Theory Tech, vol. MTT-29, pp.600-605, June 1981.

[16] B.M.A. Rahman and J.B. Davies, "Finite Element Solution of Integrated Optical Waveguides", J Lightwave Tech, vol. LT-2, no. 5, October 1984.

[17] B.M.A. Rahman and J.B. Davies, "Analysis of Optical Waveguide Discontinuities", J Lightwave Tech, vol. 6, no. 1, pp. 52-57, January 1988.

[18] S. Yamamoto, Y. Koyamada and T. Makimoto, "Normal-mode Analysis of Anisotropic and Gyrotropic Thin-film Waveguides for Integrated Optics", J Appl Phys, vol. 43, no. 12, pp. 5090-5097, December 1972.

[19] I.P. Kaminov and J.R. Carruthers, "Optical Waveguiding Layers in $LiNbO_3$ and $LiTaO_3$", Appl Phys Lett, vol. 22, no. 7, pp. 326-328, 1973.

[20] J.C. Campbell, F.A. Blum, D.W. Shaw and K.L. Lawley, "GaAs Electrooptic Directional Coupler Switch", Appl Phys Lett, vol. 27, no. 4, pp. 202-205, 1975.

[21] W.J. English and F.J Young, "An E-vector Variational Formulation of Maxwell's Equations for Cylindrical Waveguide Problems", IEEE Microwave Theory Trans, vol. MTT-19, pp. 40-46, January 1971.

[22] Private communication with Kate Remley, Oregon State University.

APPENDIX 1

APPENDIX 1

DETAILS OF THE FINITE ELEMENT PROGRAM

The finite element program used in the above analysis is available with the authors, Gannavaram D. Vishakhadatta and Dr. Tom Plant. The routines were written in Fortran. The program used the CG eigen value extraction routine from Netlib, by J.J. Dongarra. The inputs required are the dimensions of the waveguide and the refractive indices of the cover, waveguide and substrate layers. The assumed decay lengths in the cladding layers also need to be input. The output consists of the effective indices of the eigen modes and their field distributions. The presence of different modes can be studied by observing the field distribution patterns.

The program was usually run with a discretization of 20 nodes. At this level of discretization the program occupied at most 3 MB of RAM and took roughly 55 seconds to calculate the effective indices of propagating modes at a given value of β on an Apollo workstation. In order to check the accuracy of the program, it was also run with 50 nodes for the single mode waveguide cases. The variation in the results observed was insignificant (in the order of 1.0×10^{-4}). Table A1.1 shows the convergence in the values of the effective index, N_{eff}, predicted by the finite element program for the TE0 and TM0 modes of the single mode waveguide of thickness 3000 Å as a function of the number of nodes chosen in the problem. The error in the discretization approximation tails off to a very low value when we choose to use more than 12 nodes.

Number of nodes used in the problem discretization	Effective Index of the TE0 mode (Exact N_{eff} = 1.6773)	Effective Index of the TM0 mode (Exact N_{eff} = 1.634)	Simulation time per N_{eff} calculation (seconds)
5	1.615	1.587	4
8	1.633	1.622	11
12	1.634	1.634	21
20	1.657	1.634	55
50	1.657	1.634	180

Comparison of convergence in effective index values with various discretizations of the finite element problem

TABLE

A1.1